Clays and Clay Minerals, Vol. 56, No. 2, 222–243, 2008.

SPATIAL AND TEMPORAL EVOLUTION OF HYDROTHERMAL ALTERATION AT LAVRAS DO SUL, BRAZIL: EVIDENCE FROM DIOCTAHEDRAL CLAY MINERALS

EVERTON MARQUES BONGIOLO[1,3,*], PATRICIA PATRIER-MAS[2], ANDRÉ SAMPAIO MEXIAS[3], DANIEL BEAUFORT[2], AND MILTON LUIZ LAQUINTINIE FORMOSO[3]

[1] CPRM, Geological Survey of Brazil, Rua Banco da Província 105, 90840-030, Porto Alegre, RS, Brasil
[2] Université de Poitiers, CNRS, HYDRASA, 40 Avenue du Recteur Pineau, 86022 Poitiers, France
[3] Universidade Federal do Rio Grande do Sul, UFRGS, Instituto de Geociências, Av. Bento Gonçalves 9500, 91509-900, Porto Alegre, RS, Brazil

Abstract—The Au-Cu (±Pb, Zn, Ag) prospects of Lavras do Sul, southernmost Brazil, are hosted in Neoproterozoic granitic and volcanogenic rocks. Mineralization occurs in structurally controlled N40ºW to E−W quartz veins; sericite (±chlorite) and sulfides are the main secondary minerals in associated wall rocks.

In the present contribution we use petrography (optical microscopy and scanning electron microscopy (SEM)), mineralogy (X-ray diffraction (XRD) with polytypes, FWHM, decomposition of diffraction patterns), and crystal chemistry of samples from several prospects to document the spatial and temporal evolution of sericitic alteration of veins and wall rocks associated with gold.

Hexagonal, coarse-grained $2M_1$ phengite-rich alteration (± illite) is best developed with coarse-grained primary growth (comb) quartz + pyrite ± Au veins and altered wall rock from the western portion of the granitic complex (phyllic alteration). Pure phengite was recognized by narrow XRD profiles (FWHM $\leqslant$0.2º2θ CuKα) of the <5 μm particle-size fraction, non-expandable d_{001} X-ray reflections and interlayer charge (IC) >0.9 per $O_{10}(OH)_2$.

Towards the eastern zones of the granitic complex and in the volcanogenic rocks, wider XRD profiles (FWHM values $\geqslant$ 0.2º2θ CuKα) were decomposed. They contain mixtures of coarse- to fine-grained, lath-like crystals of both $2M_1$ and $1M$ illite (non-expandable d_{001} X-ray reflections, IC between 0.85 and 0.89 per $O_{10}(OH)_2$) with expandable d_{001} reflections associated with lath-like, fine-grained crystals of ordered ($R \geqslant 1$) illite-rich I-S (80−90% of illite; IC of ~0.8 per $O_{10}(OH)_2$), and minor amounts of regularly ordered ($R = 1$), illite-rich I-S mixed layers (75% of illite; IC of ~0.74 per $O_{10}(OH)_2$). The dioctahedral clay association of illite + illite-rich I-S mixed layers (intermediate argillic alteration) is best developed in quartz + pyrite ± Au veins, breccias, and wall-rock alteration from the eastern portion of the granitic complex and in the volcanic area. Quartz from veins and breccias has fine-grained primary growth, recrystallization, and replacement textures, similar to those in epithermal deposits.

The overall distribution of the dioctahedral clays indicates that the study area represents a fracture-controlled, tilted, porphyry to epithermal deposit, with telescoping alteration features observed in the east of the mining district. Deeper levels of exposure of a large hydrothermal system are observed in the west of the mining district, as shown by higher-rank dioctahedral minerals (phengite) that crystallize at relatively high temperatures ($T_{phe} \approx$ 300ºC, phyllic alteration) associated with coarse-grained, primary-growth quartz veins, similar to those observed in porphyry deposits. On the other hand, shallower levels of exposure are observed in the east of the study area, associated with abundant, lower-rank dioctahedral clay minerals (illite + illite-rich I-S mixed layers, intermediate argillic alteration) that crystallize at relatively lower temperatures ($T_{I\text{-}S} \approx$ 120−200ºC).

Available data show that gold is associated with phengite, but that lower-rank, overprinting alteration characterized by illite-I-S may have locally modified the original gold grades.

Key Words—Brazil, Clay Minerals, Gold, Hydrothermal Alteration, Illite, Lavras do Sul, Mixed-layer Illite-smectite, Phengite, Polytypes, Prospects, X-ray Diffraction.

INTRODUCTION

Located in the Rio Grande do Sul state, southernmost Brazil (Figure 1a), the Lavras do Sul Au-Cu (±Pb, Zn, Ag) mining district comprises a group of prospects hosted in Neoproterozoic granitic and volcanic rocks. Several investigations of gold prospects were conducted in this district by Brazilian public agencies in the 1940s and between 1974 and 1995. They estimated gold resources of ~3.5 t, 6 t, and 7.5 t for the Cerrito, Bloco do Butiá, and Volta Grande prospects, respectively (Figure 1b, locations 8, 19, and 2, respectively). New exploration programs by mining companies are now underway to re-evaluate these reserves.

Some work has been conducted on the alteration and mineralization features by Mexias *et al.* (1990, 2005), who suggested that the Lavras do Sul Intrusive Complex

* E-mail address of corresponding author:
ebongiolo@pa.cprm.gov.br
DOI: 10.1346/CCMN.2008.0560207

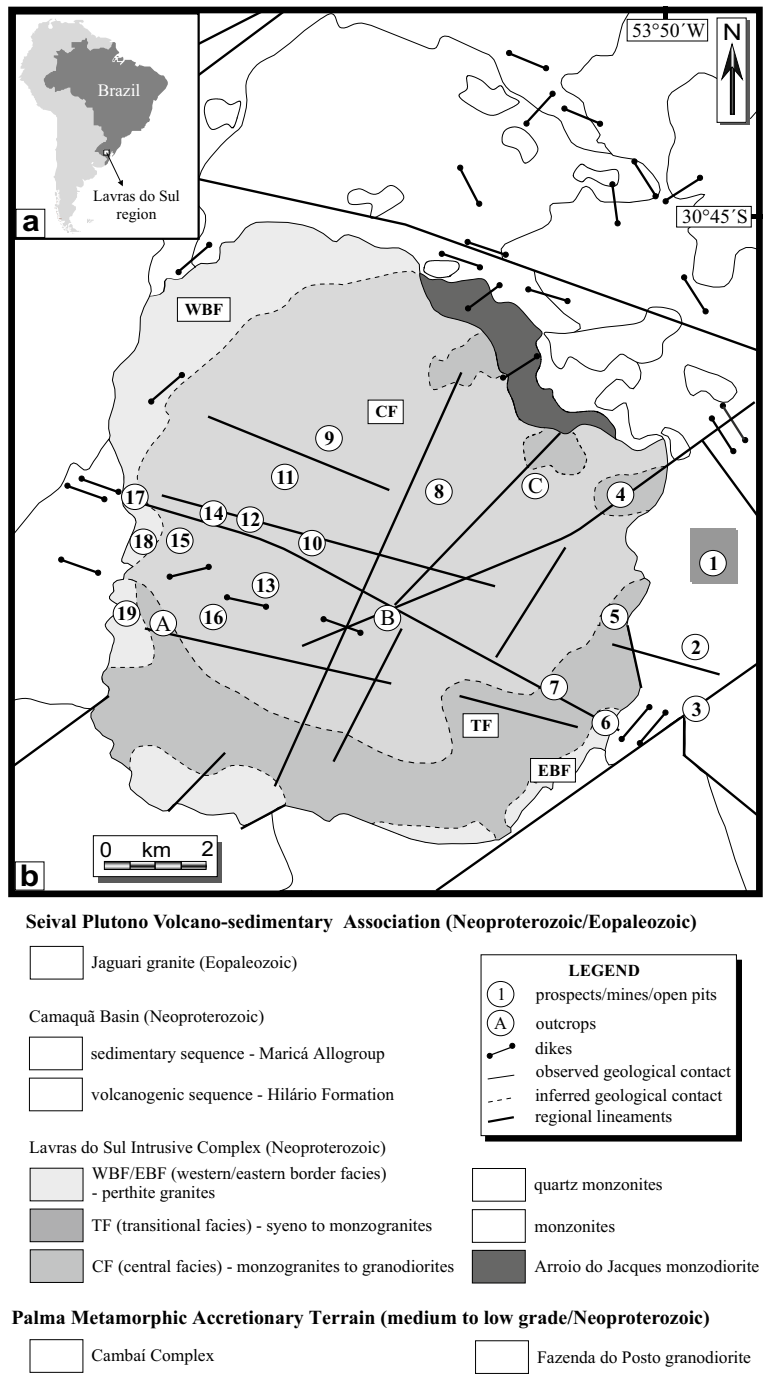

Figure 1. (a) Map of South America showing the location of the study area. (b) Simplified geological map of the Lavras do Sul region, modified after Reischl (1980) and Gastal and Lafon (1998). Prospects: (1) Cerro Rico; (2) Volta Grande; (3) Saraiva; (4) Dourada; (5) Aurora; (6) Valdo Teixeira; (7) Mato Feio; (8) Cerrito; (9) Santo Expedito; (10) Paredão; (11) Pitangueira; (12) Olaria; (13) São José; (14) Taruman; (15) Caneleira; (16) Virgínia; (17) Zeca Souza; (18) Galvão, and (19) Bloco do Butiá. Sampling was performed in all prospects except for locations 3, 10, 11, 14, and 15 and in outcrops (A, B, and C).

acted as a source of heat in the production and the persistence of a large hydrothermal system. In the Volta Grande area: (1) a fracture-controlled K-feldspar + biotite + tourmaline + allanite + chalcopyrite (± cross-cutting adularia) early assemblage predated (2) the pervasive crystallization of chlorite + epidote + calcite assemblage; and (3) the vein-controlled crystallization of sericite + quartz + pyrite ± chlorite. The final alteration stage (4) consisted of vein-controlled carbonates + hematite + corrensite + sericite assemblage. The

https://doi.org/10.1346/CCMN.2008.0560207 Published online by Cambridge University Press

aforementioned assemblages are similar to the (1) potassic, (2) propylitic, (3) phyllic, and (4) argillic alteration reported in porphyry copper deposits by several authors (Creasey, 1959; Lowell and Guilbert, 1970; Beane, 1982).

Phyllic, intermediate argillic, and argillic alteration may crystallize the quartz-sericite-pyrite assemblage in veins; these veins begin to develop contemporaneously with propylitic alteration (convective heat flow), but the major discharge of fluids in fracture zones takes place during decreasing heat conduction stages of hydrothermal systems (Norton and Knight, 1977). Quartz-sericite-pyrite veins and associated alteration halos are the main host for gold in the study area (Kaul and Reinheimer, 1974), existing as "invisible gold" in pyrite grains (Mexias *et al.*, 2005).

Sericite is a generic term based on petrographic observations. It is commonly used for all the fine-grained potassic dioctahedral phyllosilicates that coexist or are spatially associated in hydrothermally altered rocks. However, the term includes different types of swelling and non-swelling clay minerals that did not necessarily crystallize at the same temperature, fluid composition, or fluid-rock ratio (Inoue, 1995; Meunier, 2003). Sericite forms as an alteration product from interaction between fractured rocks and hydrothermal fluids over a large range of thermal conditions (from 350ºC to <100ºC; Nadeau and Reynolds, 1981; Horton, 1985; Simmons and Browne, 1998; Parry *et al.*, 2002).

Clay minerals are a useful tool to recognize spatial and temporal evolution of hydrothermal systems and fluid flow paths as shown by studies of geothermal environments (Reyes, 1990; Flexser, 1991; Harvey and Browne, 1991; Patrier *et al.*, 1996; Bril *et al.*, 1996; Mas *et al.*, 2003). In porphyry deposits, several generations of sericite occur successively near the transition between the mesothermal (phyllic alteration) and the shallower epithermal hydrothermal environments (argillic alteration), with common overprinting features. The alteration mineralogy of these complex systems requires a detailed study of the clay mineralogy (Jin *et al.*, 2002; Parry *et al.*, 2002; Franchini *et al.*, 2007) to make a real distinction between the dioctahedral clay minerals crystallized under phyllic, intermediate argillic, and argillic alteration conditions.

This work was motivated by the lack of detailed data on hydrothermal alteration at a regional scale in the Lavras do Sul mining district. The aims of the present contribution are: (1) to determine the textural properties, the crystal structure, and the crystal chemistry of the clay minerals that constitute the sericitic alteration related to the main Au prospects, using detailed study of alteration petrography coupled with SEM observations, X-ray diffraction, and microprobe analyses; (2) to determine the spatial and temporal evolution of the clay minerals by studying samples collected in numerous prospects representative of the whole mining district; and (3) to use mineral characteristics to estimate temperature and fluid chemistry for the clay-bearing alteration associated with minor gold deposition.

GEOLOGY

Lithology

The rocks from the Lavras do Sul district (Figure 1b) belong to the Neoproterozoic Seival Association which consists of a volcano-sedimentary sequence (Camaquã Basin) intruded by granitic rocks in a foreland tectonic setting, associated with the subduction of the Kalahari plate under the Rio de La Plata plate (Chemale *et al.*, 1995).

The local granitic complex that hosts the Au mineralization is characterized by a reverse zonation of its geochemical affinity and petrographic textures, called central, transitional, and border facies (Nardi, 1984). The central facies (CF) contains shoshonitic rapakivi coarse-grained granodiorites and monzogranites with porphyritic to serial heterogranular texture and Fe-edenite and Fe-biotite as mafic mineral phases. The border facies (BF) has coarse-grained equigranular perthitic alkaline granites with Fe-edenite to Fe-hornblende (±Fe-biotite) and locally porphyritic biotite syenogranites, which occur in the periphery (western and eastern border facies – WBF and EBF, respectively) of the central facies. The transitional facies (TF) consists of texturally and geochemically hybrid rocks (monzo and syenogranites) generated by partial assimilation of the central zone by the border zone (Nardi, 1984). Gastal and Lafon (1998) proposed the term Lavras do Sul Intrusive Complex (LSIC), which includes monzodiorites and hypabyssal porphyritic monzonites and quartz monzonites to the major granitic complex. U-Pb SHRIMP zircon data give an age of 594±5 Ma (Remus *et al.*, 2000) for both central- and border-facies granitoids.

The granitic complex intruded both the metamorphic Cambaí Complex (~750–700 Ma; Babinski *et al.*, 1996) and the Hilário Fm (~600Ma; Remus *et al.*, 2000), a basic to intermediate volcanogenic sequence, producing hornblende to albite-epidote hornfels in the latter (Ribeiro, 1983; Mexias *et al.*, 1990). The volcanogenic rocks (~600 Ma), which also host hydrothermal veins, include lithic-, crystal-, ash-, and lapilli-tuffs, agglomerate, and pyroclastic breccia, interlayered with trachybasalts and trachyandesites, epiclastic deposits, and minor ignimbrites (Lima and Nardi, 1998). Dikes of highly variable compositions (lamprophyres, minnetes, rhyolites), as well as subvolcanic monzonites, intrude both the granitic complex and the volcanogenic sequence (Lima and Nardi, 1998; Gastal *et al.* 2003; De Liz *et al.* 2004) and evidence of coeval basic and acid magmatism are supported by the presence of microgranular mafic enclaves in the granitic complex (Nardi and Lima 2000).

https://doi.org/10.1346/CCMN.2008.0560207 Published online by Cambridge University Press

Structural features

Regional lineaments coincide with the occurrence of altered and mineralized zones in the granitic and volcanogenic rocks. In the Lavras do Sul district, the major gold deposits occur in veins and breccias that strike N40ºW to E–W in most places, and locally NE–SW (Figure 1b). Preliminary structural data show that these veins and breccias are associated in the field with right-lateral (NE–SW) and left-lateral (NW–SE) strike-slip brittle faults. NW–SE faults are comparatively younger than NE–SW ones.

MATERIALS AND METHODS

Eighty two samples of altered rocks were collected at surface outcrops, open pits, and exploration drill cores (Table 1). Sampling focused on sericite-rich veins and their related alteration halos because they are the main host for gold in all the prospects of the study area. The alteration petrography and mineralogy of these veins, and wall-rock alteration is described in the following sections. The sampling was carried out in such a way as to ensure that we obtained representative surface distribution of the hydrothermal alteration stages (veins and wall rock) including sericite (+ sulfides ± ore) in both the granitic complex and from the surrounding volcanogenic rocks. Samples collected from surface outcrops and affected by weathering were identified and excluded from this study.

Samples from exploration drill cores and its associated ore contents were provided by Brazilian public agencies (Companhia de Pesquisas de Recursos Minerais – CPRM, Companhia Riograndense de Mineração – CRM, and Companhia Brasileira do Cobre – CBC). Those ore contents were compared with the clay mineralogy in the same samples to evaluate whether there is a specific and/or preferred assemblage associated with ore crystallization. Samples collected in veins and wall rocks from the WBF (BB samples, location 19) and the CF (CF samples, location 8) have between 1 and 1.5 g/t of Au. Samples from the EBF (VT samples, location 6) contain an average of <0.3 g/t of Au (locally 1.2 to 2.3 g/t) and <0.02% of Cu (locally up to 1.3%) in veins and wall rocks. Samples from the volcanic rocks (FVG samples, location 2) have an average 3 g/t of Au and 1.2% of Cu. Data available in the literature (Kaul and Reinheimer, 1974; Reischl, 1998) show that average ore contents in veins and wall rocks from the study area are <2.5 g/t of Au and <0.02% of Cu in the prospects hosted by granitic rocks (WBF, CF, TF, and EBF, locations 4–19) and up to 3 g/t of Au and 1.2% of Cu in the volcanogenic area (locations 1–3). However, the larger ore-content values in all prospect areas are typically associated with supergene enrichment.

A sequence of four samples was selected within a 30 cm wide alteration halo related to a 1 cm-wide quartz vein (Table 1; samples VT2-63.5 to 63.8m) crosscutting a porphyritic granitic rock from EBF, in order to study the variation of crystal structure and chemical features of the dioctahedral phyllosilicates as a function of increasing distance from the vein.

Petrographic observations of hydrothermal alteration were performed on thin sections using a Leica DMLP optical polarizing microscope, coupled with a digital Sony Exwave HAD photographic camera. A scanning electron microscope (SEM – Jeol JSM 5800) was used to examine the particle morphology of clay minerals in altered rock fragments covered with carbon.

The crystal structures of the clay minerals were identified using XRD techniques. The XRD analyses of all samples were performed in air-dried (AD) and ethylene glycol-saturated (EG) states with oriented preparations. The samples were initially crushed gently under distilled water and the fragments were put in contact with $N_{2\ (liquid)}$ to disaggregate the clay-size material from rocks. Samples were dispersed ultrasonically in distilled water and the <5 μm size fractions were extracted from the suspension obtained after 20 min of sedimentation. The clay suspension was then vacuum filtered through a millipore filter (pore diameter: 0.08 μm) and the filter was placed face down on a glass slide. This method produces mounts that have good crystallite orientations and give reproducible intensities (Bish and Reynolds, 1989). A Philips PW1729 diffractometer ($CuK\alpha_{1+2}$ radiation, 40 kV, 40 mA) equipped with a stepping-motor drive in the goniometer was used to obtain the XRD data. The divergence slit, receiving slit, and scatter slit were 1º, 0.1 mm, and 1º, respectively. Motor and intensity acquisition commands were made using a Socabim DACO MP device and the data treatment was performed using the DIFFRAC AT software. The data were acquired in the 2–30º2θ range with a step size of 0.02º2θ and a counting time of 3 s per step.

The full width at half maximum intensity (FWHM) of d_{001} reflections was measured using the DIFFRAC AT software in all oriented diffraction patterns (AD and EG), to obtain a comparative crystallinity index. The FWHM is associated with the number of layers that diffracts in a coherent form (CSDS: coherent scattering domain size along the c^* axis), *i.e.* the narrower the d_{001} peaks (lower FWHM value), the greater the CSDS value (Meunier and Velde, 2004). The initial distinction between dioctahedral clay minerals using the FWHM criterion was as follows: peaks with $\leqslant$0.2º2θ $CuK\alpha$ FWHM values that do not change position after EG solvation were classified as phengite/mica (Bouchet *et al.*, 2001); peaks with $\geqslant$0.2º2θ $CuK\alpha$ FWHM values that do not change position after EG solvation were classified as illite and those that do change position (presence of expandable phase) were classified as I-S mixed layers. Smectite layers in illite-rich I-S mixed layers tend to widen the basal spacing peak and shift it to

https://doi.org/10.1346/CCMN.2008.0560207 Published online by Cambridge University Press

Table 1. Location and characteristics of samples used in this study. All samples analyzed from veins are of type 1 (see text).

Sample	Host rock	Location (prospect)	Characteristics	FWHM AD-EG	Sample	Host rock	Location (prospect)	Characteristics	FWHM AD–EG
A1	VR	2	pervasive alteration (chl rich)	0.31–n.d.	*VT5-26.5mB*	EBF	6	wall rock alteration (ser + chl)	1.12–0.77
A7	TR	2	pervasive alteration (chl rich)	0.18–0.24	*VT6-45.6m*	EBF	6	wall rock alteration (chl + ser rich)	0.49–0.40
CT45A	VR	2	qtz + ser + py + cpy vein selvage	0.45–0.44	CT26B	EBF	6	qtz + ser + py vein selvage	0.55–0.51
CT51B	VR	2	wall rock alteration (chl rich)	0.34–0.25	CT66A	EBF	4	qtz + ser + py vein selvage	n.d.–0.77
CT71C	TR	2	qtz + ser vein selvage	0.29–0.29	CT66B	EBF	4	wall rock alteration (ser rich)	0.72–0.69
CT71D	TR	2	pervasive alteration (chl rich)	0.58–0.61	CT69B	EBF	6	wall rock alteration (3m-ser rich)	0.76–0.58
CT71J	TR	2	pervasive alteration (chl rich)	0.47–0.41	CT69C	EBF	6	wall rock alteration (2.5m-ser rich)	0.84–0.54
FVG-384-21m	TR	2	qtz +ser +sulf ±Au-Cu stockwork	0.20–0.18	CT69D	EBF	6	wall rock alteration (2m-ser rich)	0.68–0.52
FVG-484-32m	TR	2	qtz +ser +sulf ±Au-Cu stockwork	0.31–0.33	CT69E	EBF	6	wall rock alteration (3.5m-ser rich)	0.82–0.64
FVG-384-44m	VR	2	qtz + ser + py vein/breccia	0.20–0.20	CT69F	EBF	6	qtz + ser + py vein selvage (5cm)	0.80–0.58
E017G	VR	-	wall rock alteration (?)	0.31–0.26	CT69G	EBF	6	qtz + ser + py vein selvage	0.71–0.59
E32C	VR	-	pervasive alteration (chl rich)	0.44–n.d.	CT69H	EBF	6	wall rock alteration (ser rich)	0.71–0.66
DOU-P	EBF	4	qtz + ser + py vein/breccia	0.76–0.69	CT69I	EBF	6	qtz + ser + py vein selvage	0.71–0.67
AUR-B	EBF	5	qtz + ser vein	0.26–0.25	CT69K	EBF	6	qtz + ser + py vein selvage	0.68–0.59
NAUR	EBF	5	qtz + ser vein selvage	0.17–0.18	EMF-6	EBF	7	qtz + ser + py vein selvage	0.23–0.22
CT2C	EBF	5	pervasive alteration (chl rich)	0.39–0.43	EMF-1	EBF	7	qtz + ser + py vein selvage	n.d.–0.89
CT70A	EBF	5	qtz + ser vein selvage	n.d–0.36	*C.F04.86-66m*	CF	8	qtz + ser + py ± Au vein/breccia	0.23–0.23
VT2-9.2mA	EBF	6	qtz + ser + chl + py vein selvage	0.21–0.23	*C.F04.86-66.5m*	CF	8	wall rock alteration (ser + chl rich)	n.d.–n.d.
VT2-9.2mB	EBF	6	wall rock alteration (ser + chl rich)	0.57–0.53	*C.F02.84-18.4m*	CF	8	wall rock alteration (ser + chl rich)	0.65–0.53
VT2-14m	EBF	6	qtz + ser vein	0.68–0.51	CT67A	CF	-	qtz + ser vein selvage	0.85–0.63
VT2-34mC	EBF	6	qtz + ser + py + cpy vein selvage (5 cm)	0.76–0.49	CT67B	CF	-	qtz + ser vein selvage	0.42–0.41
VT2-34mD	EBF	6	qtz + cal vein	0.78–0.60	CT67C	CF	-	qtz + ser vein selvage	0.29–0.31
VT2-34mE	EBF	6	wall rock alteration (ser rich)	0.48–0.41	CT68A	CF	8	qtz + ser + py vein selvage	0.48–0.54
VT2-44.8mB	EBF	6	qtz+ser+chl+cpy+cal±Cu breccia (10cm)	0.75–0.48	CT68B	CF	8	qtz + ser + py vein selvage	0.60–0.46
VT2-52mA	EBF	6	qtz + ser vein selvage	0.70–0.52	CT68C	CF	8	qtz + ser + py vein selvage (50 cm)	0.36–0.34
VT2-52mB	EBF	6	qtz + ser vein selvage	0.86–0.63	FAZCH	CF	9	qtz + ser + py vein selvage	0.17–0.16
VT2-55mA	EBF	6	qtz + ser vein selvage	0.96–0.70	PIT-B	CF	11	qtz + ser +py vein/breccia	0.40–0.24
VT2-55mB	EBF	6	qtz + ser vein selvage	0.98–0.67	OLA-X	CF	12	qtz + ser +py vein/breccia	0.19–0.15
VT2-55mC	EBF	6	qtz + ser vein selvage	0.92–0.65	OLA	CF	12	qtz + ser + py vein/breccia	n.d.–0.81
VT2-55mD	EBF	6	qtz + ser vein selvage	0.74–0.52	SJ4	CF	13	qtz + ser + py vein/breccia	0.18–0.17
*VT2-63.5m**	EBF	6	qtz + ser vein	0.71–0.54	SJ	CF	13	wall rock alteration (ser rich)	0.38–0.31
*VT2-63.6m**	EBF	6	wall rock alteration (ser rich)	0.88–0.66	VIR	CF	16	qtz + ser + py vein selvage	0.21–0.22
*VT2-63.7m**	EBF	6	wall rock alteration (ser rich)	1.13–0.79	ZS3	WBF	17	qtz + ser + py vein selvage	0.20–0.20
*VT2-63.8m**	EBF	6	wall rock alteration (ser rich)	1.18–0.79	*BB1185-93m*	WBF	19	wall rock alteration (ser rich)	0.15–0.16
VT2-65m	EBF	6	qtz + ser + py vein selvage	0.79–0.65	*BB1185-93.1m*	WBF	19	wall rock alteration (ser rich)	0.14–0.14
VT3-22.5m	EBF	6	wall rock alteration (ser rich)	0.88–0.71	*BB1185-93.2m*	WBF	19	wall rock alteration (ser rich)	0.17–0.17
VT3-34.5m	EBF	6	qtz + ser vein selvage	1.06–0.73	*BB1185-93.3m*	WBF	19	wall rock alteration (ser rich)	0.15–0.16
VT3-35.1mA	EBF	6	qtz + ser + py + cpy vein/breccia	0.61–0.50	GAL	WBF	18	qtz + ser + py vein selvage	0.14–0.15
VT5-12.9m	EBF	6	qtz + cal vein	0.71–0.55	GAL4	WBF	18	qtz + ser + py vein selvage	0.17–0.17
VT5-26.5mA	EBF	6	wall rock alteration (ser + chl)	1.06–0.75	*BB0185-190m*	WBF	19	episyenite (ser rich)	0.19–0.18
VT3-35.1mB	EBF	6	qtz + ser + py + cpy vein/breccia	0.40–0.34	*BB1185*	WBF	19	episyenite (ser rich)	0.21–0.20

Abbreviations: qtz = quartz, WBF = western border granitoids, CF = central facies granitoids, EBF = eastern border granitoids, VR = volcanic rock and TR = tuffaceous rock. Rocks marked with * represent porphyritic rocks sampled to observe structural evolution of clays with increasing distance from a vein. The locations of the prospects correspond to those shown in Figure 1b. Full width at half maximum (FWHM) of dioctahedral clays (<5 μm) was measured at the d_{001} reflection near 10 Å on XRD profiles. Values were compared between air-dried (AD) and ethylene glycol-solvated (EG) preparations. n.d. = not determined, due to interference by another mineralogical phase. Ore contents of samples listed in *italic* were obtained from mining agencies.

higher values if the smectite is hydrated or has only one layer of glycol per smectite layer, but if the smectite layer is fully glycol-saturated (17 Å basal spacing) and the crystallites have high illite content, the peak position near 10 Å will be shifted to a spacing of <10 Å (Meunier and Velde, 2004). Peaks with FWHM values very near to 0.2º2θ CuKα that do not change position after EG solvation need further investigation (crystal chemistry, see below) to make a precise distinction between phengite/mica and illite (Bouchet *et al.*, 2001).

Some of the more complex d_{001} X-ray reflections (broad peaks and/or peaks with FWHM near the limits used to perform an initial identification of the clay components within the peak) were decomposed into elementary component curves of Gaussian form using DECOMPXR software (Lanson and Besson, 1992). After decomposition, the individual d_{001} X-ray reflections were identified and compared with simulations using *Newmod*® (Reynolds, 1985). This software was also used to estimate the percentage of illite layers and the degree of order-disorder in the stacking sequence of I-S mixed layers (R = 0, R = 1, R ⩾ 1) based on shift of the peak position of the d_{001} reflections after EG solvation on the <5 μm size fraction.

Structural parameters such as the FWHM values and the degree of order-disorder in the stacking sequence of the dioctahedral clay minerals are considered broad indicators of *P-T* conditions in geological environments, including low-grade metamorphism, diagenesis, and hydrothermal alteration (see review by Merriman and Peacor, 1999). The lower the FWHM value and the higher the order in the stacking sequence, the higher the temperature of the crystals. The same crystal structural parameters on dioctahedral clay minerals obtained in this study were compared with the available literature data to evaluate the *P-T* conditions of crystallization of clays in the Lavras do Sul area.

Polytype data were obtained from randomly oriented powder mounts of the <5 μm particle-size fraction from the samples using a Philips Panalytical X'pert Pro diffractometer. CuKα_{1+2} radiation was used (40 kV, 40 mA) and collected by an X'celerator detector. The acquisition was made in the 18–36º2θ range with a step size of 0.004º2θ. The divergence slit and scatter slit were ½º and ¼º, respectively. The peak positions obtained by XRD were compared with peak positions available in the literature (Reynolds, 1980) and with peak positions obtained by computer simulations (Drits and McCarty, 1996) for the $2M_1$ polytype, as well as for the 1*M* polytype in *cis*-(1*Mc*) and trans-(1*Mt*) vacant forms.

Petrographic and textural relationships, as well as chemical analyses of thin sections were performed using a Jeol JSM 5600LV SEM equipped with an INCA energy-dispersive X-ray fluorescence analyzer (EDS, Si(Li) semi-conductor). The samples were covered with a thin film of carbon. The standards used for EDS were albite, forsterite, orthoclase, wollastonite, manganese metal, titanium

https://doi.org/10.1346/CCMN.2008.0560207 Published online by Cambridge University Press

metal, and pyrite. The elements analyzed were Na, Mg, Al, Si, K, Ca, Ti, Mn, and Fe, and the analytical conditions were as follows: accelerating voltage 15 kV, probe current 0.60 nA and counting time 60 s. Corrections were made with an Inca XPP program and the relative error on each analysis is <1.5%. Additional chemical analyses were made using a Cameca SX 50 electron microprobe apparatus with wavelength-dispersive spectrometry (WDS). The elements analyzed were Na, Mg, Al, Si, K, Ca, Ti, Mn, and Fe, and the microprobe was calibrated using synthetic and natural oxides and silicates. Corrections were made with a Cameca PAP matrix correction. The analytical conditions were as follows: current intensity 10 nA, accelerating voltage 15 kV, spot size 1 μm, and counting time 20 s per element. The relative error on each analysis was <1% of the detected quantity, except for Na (<1.5%).

The distinction between dioctahedral clay minerals using the crystal chemistry criterion (IC = interlayer charge) was as follows: 0.9 to 1 per $O_{10}(OH)_2$ for phengite/mica, 0.85 to 0.9 per $O_{10}(OH)_2$ for pure illite (Meunier and Velde, 1989; Lanson and Champion, 1991; Środoń *et al.*, 1992) and <0.85 per $O_{10}(OH)_2$ for I-S mixed layers. Samples containing crystals with variable IC were compared with FWHM values obtained on global XRD data (<5 μm) and decomposition of XRD patterns to evaluate the coexistence of clay minerals (phengite, illite and/or I-S mixed layers) and the degree of mixture between the components in I-S mixed layers.

The descriptions of quartz vein textures follow the terminology suggested by Dowling and Morrison (1990) for quartz in hydrothermal systems (porphyry and epithermal environments): (1) primary growth (comb, massive, colloform, crustiform, and zonal) (2) recrystallization (flamboyant, feathery, and mosaic); and (3) replacement (saccharoidal and lattice-bladed).

RESULTS

Field data and alteration petrography

Hydrothermal alteration occurs in a 5 km NE–SW and 12 km WNW–ESE strip. It can be organized into two main types observed in all prospect areas during field work and from petrographic studies as: (1) pervasive replacement of the most reactive pre-existing minerals in initially poorly fractured and undeformed surrounding rocks, referred to hereafter as propylitic alteration; and (2) veins (fracture sealing) surrounded by wall-rock alteration halos, referred to hereafter as phyllic to argillic alteration.

Propylitic alteration. In the granitic complex, propylitic alteration is the first and the less intense alteration stage at a regional scale. It affects preferentially the mafic minerals, with crystallization of secondary silicates and minor amounts of pyrite. It is overprinted by phyllic to argillic vein-type alteration stages dominated by the crystallization of sericite (see below). During propylitic alteration of granitic rocks, biotite is partly to totally replaced by chlorite and pseudomorphs of amphiboles by chlorite (± calcite ± ilmenite ± quartz) are common. In CF and TF granitoids, minor amounts of epidote are observed. Plagioclase (oligoclase) is slightly sericitized and K-feldspar appears cloudy with a typical reddish color. At the EBF granitoids, albite chessboard textures were developed at a local scale. In the volcanogenic rocks, propylitic alteration is characterized by the chlorite + epidote ± calcite assemblage. Chlorite occurs as vug fillings, as an alteration product of the igneous mafic minerals (amphibole, pyroxene), and as groundmass replacement in the altered tuffaceous rocks. Epidote mostly replaced the igneous plagioclase (oligoclase to labradorite). Calcite fills vugs or occurs as disseminated patches in altered plagioclase.

Phyllic to argillic alteration. Three major types of veins have been distinguished in all the prospect areas. These veins overprint the previous propylitic alteration of their host rocks, and they are listed below in decreasing order of abundance and time of crystallization.

(1) Quartz + sericite + pyrite ± chalcopyrite ± Au disrupted veins, stockworks, and breccias (Table 1; 1 cm to 2 m wide, 3.5–500 m long) are associated with N40ºW to E–W brittle shear zones. Locally, NE–SW brittle shear zones with the same alteration assemblage are observed (locations 4, 6 and 8).

The sericite-rich veins predominate over the other vein-type alterations (see below) in the granitic rocks and are the main host for the gold deposition. In these veins, macroscopic and microscopic textures of hydrothermal quartz are highly variable and include (1) comb, massive, colloform, crustiform ± zonal; (2) ± flamboyant ± feathery ± mosaic; and (3) saccharoidal ± widespread lattice-bladed associations. Comb textures predominate in the WBF and CF granitoids, whereas very fine grained textures (colloform, crustiform and saccharoidal) predominate along the contact zones between granitic and volcanogenic host rocks. Hydrothermal breccias (quartz fragments), narrow deformational domains (quartz subgrains), microcataclasites, and intragranular fractured zones are also common in all prospect zones.

The wall-rock alteration associated with these veins is also dominated by sericite + quartz + pyrite + chalcopyrite ± Au (Table 1). Sericite occurs as veinlets, or disseminated in the rock, where it overprints the previous propylitic alteration. In some places, the vein selvages coalesce to form a more massive sericitic alteration. Bore-hole descriptions show variable extensions of alteration halos through wall rocks. The border facies granitoids (both WBF and EBF) generally contain wider alteration halos (up to 40 m) than the CF (<10 m). In the volcanogenic rocks, sericite-rich alteration halos are not easy to discern, due to the overprinting by other vein-type alteration stages (see below).

https://doi.org/10.1346/CCMN.2008.0560207 Published online by Cambridge University Press

(2) Quartz + chlorite + chalcopyrite ± pyrite ± calcite ± Cu veins, stockworks, and breccias (0.5−20 cm wide) are also associated with N40ºW to E−W brittle shear zones. These veins are widespread, but they predominate in the volcanogenic host rocks and near their contact with the EBF (locations 5 and 6), where crystallization of syntectonic chlorite and locally of lattice-bladed calcite are observed (location 6). At all localities chlorite-rich quartz veins cross cuts sericite-rich veins. The predominant quartz textures in chlorite-rich quartz veins are colloform, crustiform, zonal, and saccharoidal. Druzy/comb quartz occurs very locally.

Chlorite is abundant in the altered wall rocks. It fills microcracks, commonly in association with chalcopyrite ± pyrite. In the volcanogenic rocks and in the EBF (locations 2, 4, 5, and 6), chlorite-rich, wall-rock alteration halos are much wider (up to 1 m) than in WBF (up to 3 cm; location 19).

(3) The latest infilling stage is associated with widespread crystallization of WNW−ESE carbonate veins and veinlets (1−10 cm wide) and specular hematite in variably oriented fractures in almost all prospects. Calcite predominates in the granitic rocks, whereas dolomite predominates in the volcanogenic formations.

CHARACTERIZATION OF THE PHYLLOSILICATES

Mineralogy and petrographic relationships

Several generations of sericite were identified from the petrography of quartz + sericite + sulfide veins and their associated wall-rock alteration (Figure 2). In the WBF (locations 17 to 19), sericites from very altered zones (quartz veins and wall rock) show well crystallized forms in two major grain sizes (Figure 2a): <50 μm and between 75 and 200 μm (average 150 μm, locally up to 400 μm), but coarser crystals, which predated the smaller ones, are predominant. The SEM studies show that clay minerals in veins and altered halos have predominantly platy, sub-hexagonal to hexagonal morphology with irregular to perfect edges associated with minor amounts of very fine-grained, lath-like particles, which overgrow the hexagonal ones (Figure 2b).

In the CF, 50−100 μm sericites (average 90 μm, locally up to 150 μm) predominate in the central-west prospects. However, in the central prospects both 50−100 μm and finer (<50 μm) crystals are abundant, and different grain-size populations show clear chronological relations in zones near veins and breccias and in proximal alteration halos (Figure 2c). Fine-grained crystals grow in a later stage related to fracture fillings, where they post-date and replace coarse-grained crystals (Figure 2d). As for the WBF, larger crystals within these prospects have sub-hexagonal shapes, and the smaller crystals are lath-shaped. Within hydrothermal halos but with increasing distance from veins, alteration of magmatic biotite and feldspars also produce secondary dioctahedral phases.

In the EBF, <50 μm crystals predominate in veins and in wall-rock alteration of both equigranular perthite granites and porphyritic syenogranites (Figure 2e). Minor amounts of coarser crystals with sub-hexagonal shapes are also observed in veins (average 150 μm, up to 300 μm) and wall rocks (average 100 μm, up to 250 μm), which show clear textures of destabilization and recrystallization to finer lath-type crystals (Figure 2f,g).

In the volcanogenic rocks, chlorite is more abundant than sericite, due to greater concentration of Mg and Fe in these rocks, compared to the granitic rocks. Fine-grained sericite (<50 μm) is more abundant than the coarse-grained sericite in quartz veins and altered wall rocks. Those fine-grained minerals crystallize, usually over altered feldspar crystalloclasts (Figure 2h). Coarser crystals (75 μm up to 150 μm) are only found locally, filling vugs of volcanic rocks. Cross-cutting relations between those two grain sizes were not observed in thin sections.

Crystal structure

Sericite and chlorite coexist in most of the samples, with variable proportions due to differences in their host rock and superimposition of alteration stages. Representative XRD patterns, after EG solvation (<5 μm) of samples from both granitic and volcanogenic areas, are summarized in Figure 3.

X-ray diffraction patterns of dioctahedral micas (muscovite, phengite) and illite are characterized by basal reflections close to 10 Å, 5 Å, and 3.33 Å which are not modified after ethylene-glycol treatment. Such phyllosilicates have large CSDS values in the c^* direction (Meunier and Velde, 2004).

For true micas, high CSDS values yield low FWHM values (0.14 to 0.2º2θ CuKα) measured on <5 μm XRD patterns of several samples (Table 1). These mineral phases dominate in the WBF and in western prospects of the CF, and only minor amounts occur in other granitic (EBF and in western CF prospects) and volcanogenic zones (Figure 4a). Illite is identified by comparatively lower CSDS (Bouchet *et al.*, 2001). It is indicated in all host rocks by FWHM values of between 0.22 and 0.3º2θ CuKα (Table 1; Figure 4a). Among the more complex peaks, several differences were observed in both position and peak profiles measured on d_{001} reflections after EG solvation, which indicates the occurrence of variable amounts of expandable illite-smectite (I-S) mixed layers (Reynolds, 1980). Those peaks are usually found in samples from the CF and the EBF, and from volcanogenic rocks (Figure 4a, Table 1).

With XRD methods of mineral identification, even very small smectite contents within a single phase disqualify the material from being an illite (Meunier and Velde, 2004). In most samples, I-S compositions,

https://doi.org/10.1346/CCMN.2008.0560207 Published online by Cambridge University Press

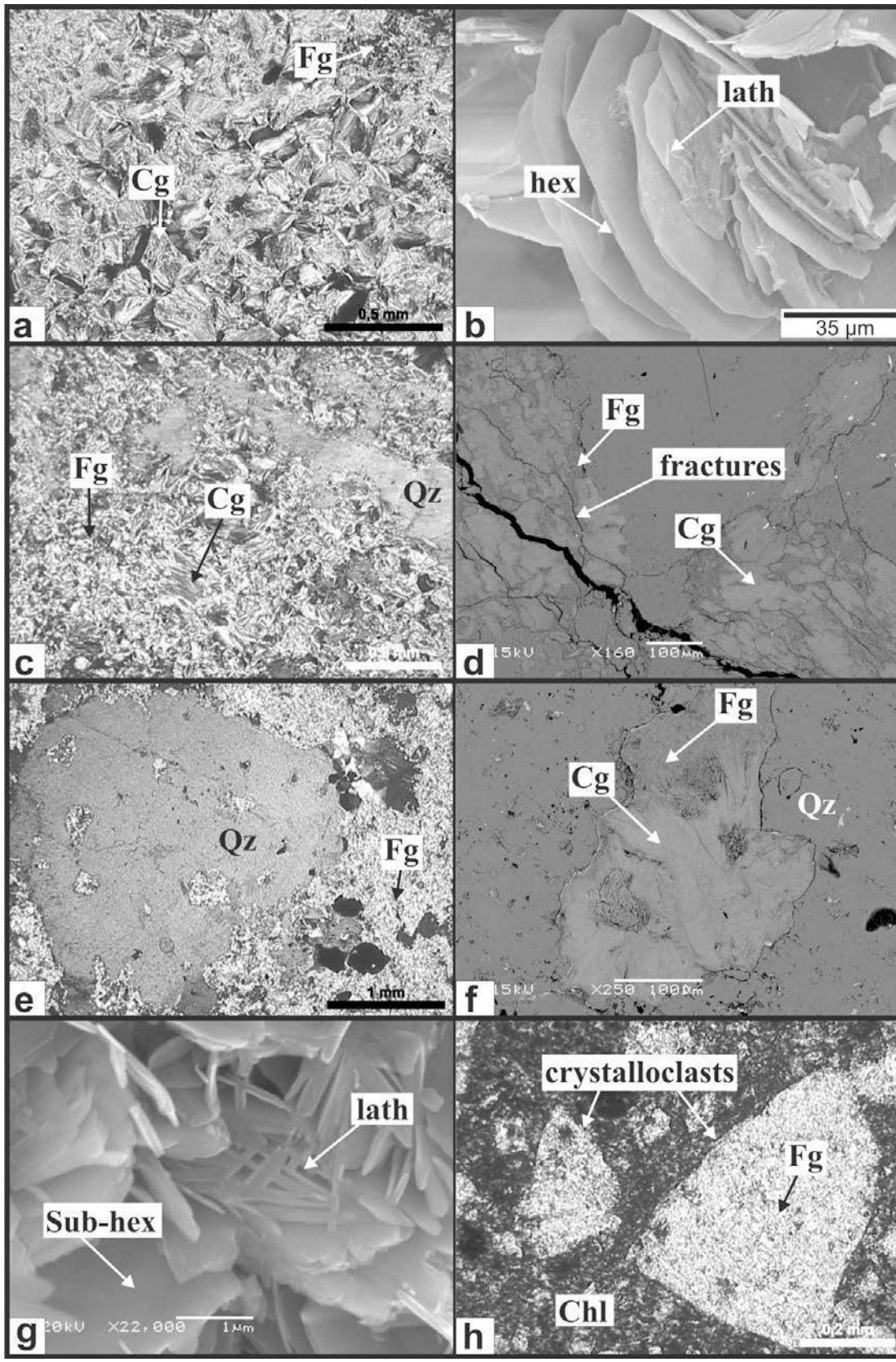

https://doi.org/10.1346/CCMN.2008.0560207 Published online by Cambridge University Press

estimated initially by comparison of the XRD patterns with simulations from the Newmod® software (Reynolds, 1985), were coherent with ordered ($R \geqslant 1$) mixed-layer structures with high illite contents (>80%) and locally (two samples) with regularly ordered ($R = 1$) ones. Samples rich in I-S mixed layers show broader peaks with FWHM values ranging from 0.29 to 1.18º2θ CuKα (Table 1; Figure 4a).

Decomposition of XRD patterns. Decomposition of XRD patterns (>99.5% fits) allows the identification of individual phases associated with the profiles of d_{001} reflections observed under <5 μm XRD examination (Figure 3). The proposed decompositions are those obtained with the minimum number of elementary components. The agreement between AD- and EG-pattern decompositions were controlled systematically. The existence of very wide peaks with low intensity, observed on some decompositions, suggests the possible existence of more complex clay associations, including additional structures (in very minor amounts) or some problems of background stepping during the decomposition process. In spite of these small uncertainties, the decomposed patterns allow better determinations of the crystal structure of each main component constituting the present clay populations of dioctahedral potassic clay minerals. Because of the good homogeneity of the results in different host rocks, further investigation was focused on representative XRD profiles (Figure 5). However, decomposed peaks with FWHM values near 0.2º2θ CuKα measured previously on <5 μm XRD diffractograms (*i.e.* samples CF04.86−66m and VT2-9.2mA), have been correctly identified as phengite/mica or as illite only after chemical analyses of those samples (crystal chemistry, see below).

Dioctahedral minerals in alteration halos, veins and episyenite vugs from the WBF (Figure 5a; sample BB1185−93.1m) mostly show narrow XRD profiles (<0.2º2θ FWHM). They were associated, after decomposition, with phengite/mica, and eventually with subordinate contents of illite. No expandable phase was observed, and the presence of illite yields a slight increase in the FWHM measured on the <5 μm XRD profiles.

In samples from the CF, different XRD profiles are associated with other elementary phases. In the western prospects of the CF, patterns with narrow basal reflections (<0.2º2θ FWHM) with no expandable phases predominate in veins and wall rocks. Towards central zones of the same granitic facies, narrow basal reflections (near 0.2º2θ FWHM; sample CF04.86−66m) also occur in veins (Figure 5b; sample CF04.86−66m) but in general the FWHM values of dioctahedral clays measured in global XRD profiles increase, due to the presence of different components in the same XRD pattern: non-expandable phengite/mica/illite and I-S mixed layers. Ordered I-S mixed layers ($R \geqslant 1$) rich in illite (80−85%) from vein selvages and alteration halos (Figure 5c, d; samples CF04.86−66.5m and CF02.84−18.4m) are characterized by broad XRD profiles with peaks positioned between 11.22 Å and 10.7 Å on decomposed AD XRD patterns. After ethylene-glycol saturation, those peaks duplicate and are positioned to the left and to the right of the primary 10 Å peak (Lanson and Besson, 1992). The distance (Å) between the first and second peaks increases progressively with increasing smectite content. Regularly ordered I-S mixed-layer minerals ($R = 1$, containing up to 75% of illite) in vein selvages and alteration halos are characterized by a large superstructure close to 25−26 Å and by broad and complex XRD profiles around 12 Å (Figure 5e; sample CT66A) in the AD state. After EG saturation, the basal reflections shift to ~27−29 Å, 13−12.5 Å, and 9.6−9.8 Å.

In most samples from the EBF, illite is ubiquitous (10 Å), but the XRD patterns show two components of ordered I-S mixed layers ($R \geqslant 1$) with large illite contents (>85%) characterized by broad peaks on AD preparations, positioned between 11 and 10.4 Å with decreasing smectite contents. After EG saturation, those peaks also duplicate and are positioned around the primary 10 Å peak. With increasing distance from a vein (location 6, from sample VT2-63.5 to 63.8m), the intensity of the illite component shows a slight decrease, relative to I-S mixed layers, coupled with broadening of each elementary peak (higher FWHM value) observed after decompositions (Figure 6a−c).

At the EBF, 10 Å reflections with small FWHM values (0.2º2θ) are observed only locally for vein samples (Figure 6d). They are associated mostly with non-expandable mica/phengite and illite, with minor amounts of ordered I-S mixed layers with high illite contents (90 to 95%).

Figure 2 (*facing page*). Textural and morphological characteristic of dioctahedral minerals as observed using optical microscopy (a, c, e, h) and SEM in secondary-electron (b, g) and backscatter (d, f) modes. Samples: (a) coarse- (Cg) and fine-grained (Fg) sericite from wall-rock alteration at the WBF (sample BB1185-93.1m); (b) coarser crystals with perfect hexagonal (hex) shapes and finer crystals with lath-like shapes from episyenites at the WBF (sample BB1185); (c) coarse- (Cg) and fine-grained (Fg) sericite in vein selvage from CF (sample CF04.86-66.5m); (d) coarse-grained (Cg) sericite cut by fractures with fine-grained (Fg) sericite in a quartz vein selvage from CF (sample CF04.86-66.5m); (e) fine-grained (Fg) sericite crystallized in porphyritic rocks from eastern border granitoids (sample VT2-63.6m); (f) coarse-grained (Cg) sericite destabilized in its borders by fine-grained (Fg) sericite in a quartz vein selvage from the EBF (sample VT2-9.2mA); (g) coexistence of sub-hexagonal and lath-like sericite particles in wall-rock alteration from the EBF (sample VT2-9.2mB); (h) fine-grained (Fg) sericite altering feldspar crystalloclasts in vein selvage from tuffaceous rock (sample FVG-484-32m).

https://doi.org/10.1346/CCMN.2008.0560207 Published online by Cambridge University Press

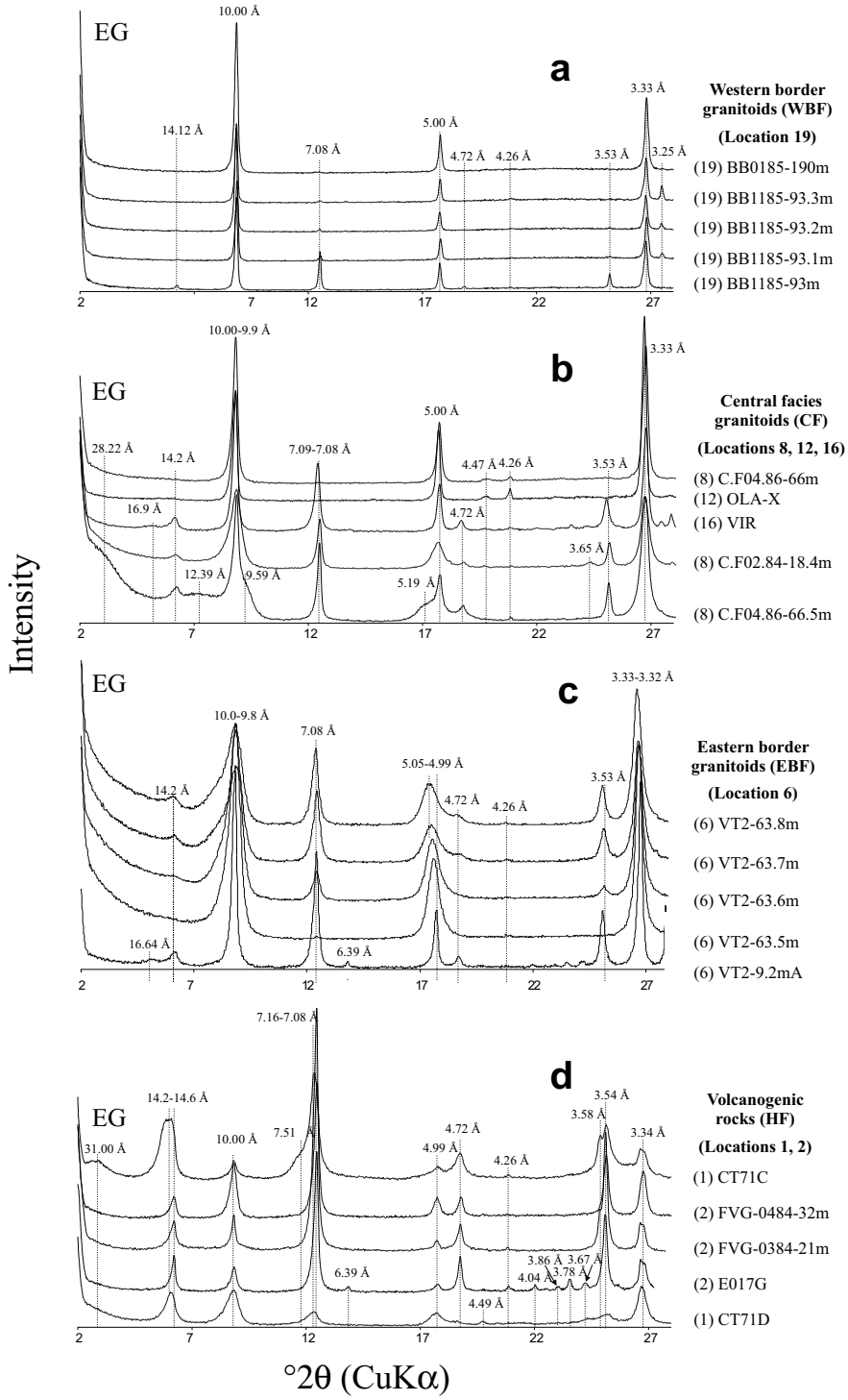

Figure 3. Representative XRD patterns of oriented powder mounts of clay minerals (<5 μm particle-size fraction) observed in veins and associated alteration halos. (a) Narrow 10 Å peaks predominate in the WBF; (b) at the CF, narrow 10 Å peaks predominate, but locally, broader peaks with variable profiles are also observed; (c) in the prospects from the EBF, broader 10 Å peaks predominate, and narrower ones are only observed locally; (d) in the volcanogenic area, sericite contents are subordinate when compared to chlorite. However, 10 Å peaks of medium width predominate over narrower and broader peaks. EG = ethylene-glycol solvated preparations.

https://doi.org/10.1346/CCMN.2008.0560207 Published online by Cambridge University Press

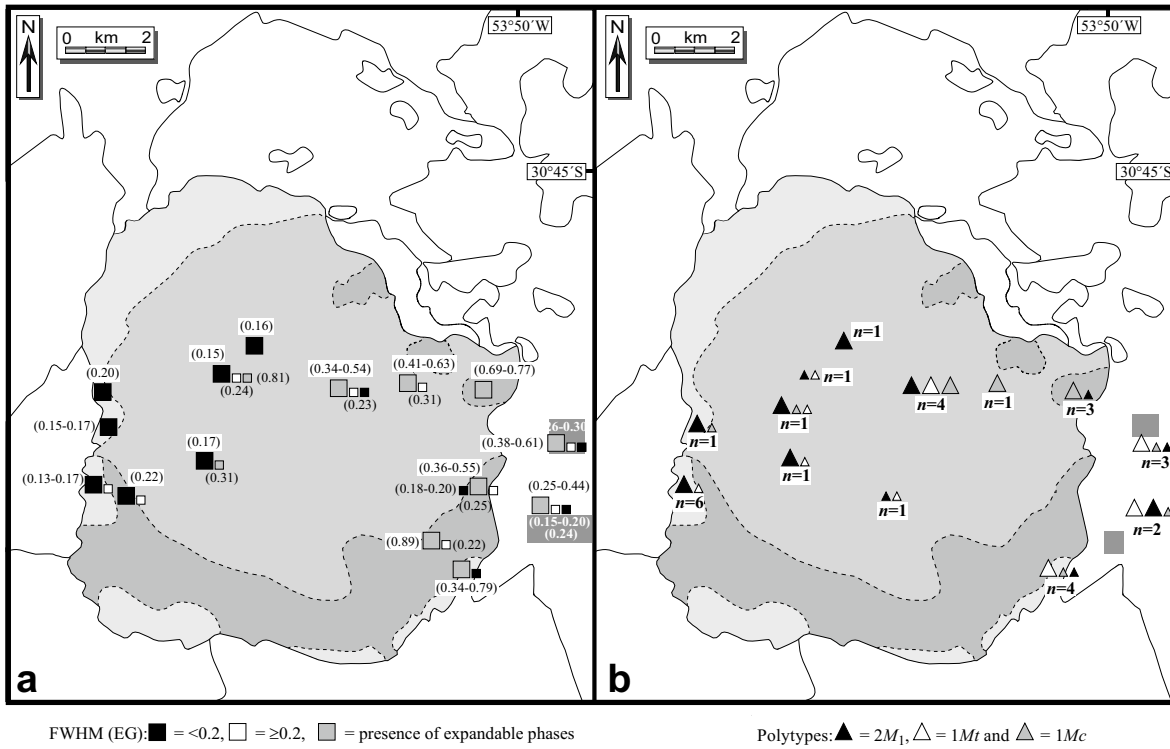

Figure 4. Summary of spatial distribution of the FWHM: (a) measured from the XRD profiles of the <5 μm particle-size fraction (see Table 1) and polytypes; (b) measured on the <5 μm fraction (see Figure 7) of representative samples within the prospect zones. The sizes of the symbols correspond to the comparative abundance of the observed parameters between samples/groups of samples. *n* = number of determinations.

Most dioctahedral phases analyzed in veins and wall-rock alteration from the volcanogenic area comprise XRD profiles of illite populations with variable CSDS (Figure 6e). Mixed-layer I-S (R ⩾ 1) with large illite contents (~90%) characterized by broad basal reflections (>0.4º2θ FWHM) occur in minor amounts in samples from veins and associated wall-rock alteration**.** Phengite/mica (basal reflections <0.2º2θ FWHM) locally fill vugs of volcanic rocks near veins and fractures.

Determination of polytypes. The spatial distribution of polytypes obtained on selected samples is summarized in Figure 4b. Despite of the presence of mineral impurities (quartz, chlorite, carbonate, and feldspars), most of the *hkl* reflections of dioctahedral minerals may be identified on XRD patterns from randomly oriented powder mounts (Figure 7). Most samples contain mixtures of $2M_1$ and 1*M* polytypes identified by offset of their diagnostic peak positions (Drits and McCarty, 1996). Veins and alteration halos from the WBF granitoids containing hexagonal coarse-grained phengite/mica/illite are characterized mainly by well defined peaks of the $2M_1$ polytype (Figure 7a). Towards CF granitoids, samples from quartz veins and breccias (Figure 7b) contain mixtures of $2M_1$ and 1*M* (*trans*- and *cis*-vacant) polytypes with $2M_1$ the predominant one (hexagonal, coarse-grained > lath-like, fine-grained crystals), whereas in samples from vein selvages and wall-rock alteration within the same zone, 1*M* polytypes predominate in the mixtures (lath-like, fine-grained > hexagonal, coarse-grained crystals) (Figure 7c). Samples from EBF and volcanic rocks (Figure 7d, e), where lath-like, finer crystals predominate, are characterized mainly by increasing amounts of the 1*M* polytype. Even if XRD reflections of finer crystals are intensified on randomly oriented powder mounts, the $2M_1$ polytype diagnostic peaks are better observed in samples from the western zones of the study area than in samples from eastern zones (Figure 4b, Figure 7).

Crystal chemistry

The average chemical compositions of sericite from veins and related alteration haloes confirm the heterogeneity of clay populations observed from petrography, XRD analyses, and decomposition of XRD patterns (Table 2, Figure 8).

The chemical compositions of the coarse-grained, dioctahedral phyllosilicates observed in the WBF vary mostly along the muscovite-phengite solid solution (Figure 8a; sample BB1185−93.1m from wall rock and epysienites). Phengites are characterized by a mean IC of 0.94 per $O_{10}(OH)_2$ (Table 2; row 1), which is typical of micas (IC = 1), essentially associated with potassium and with a negative charge of the octahedral sheet close

https://doi.org/10.1346/CCMN.2008.0560207 Published online by Cambridge University Press

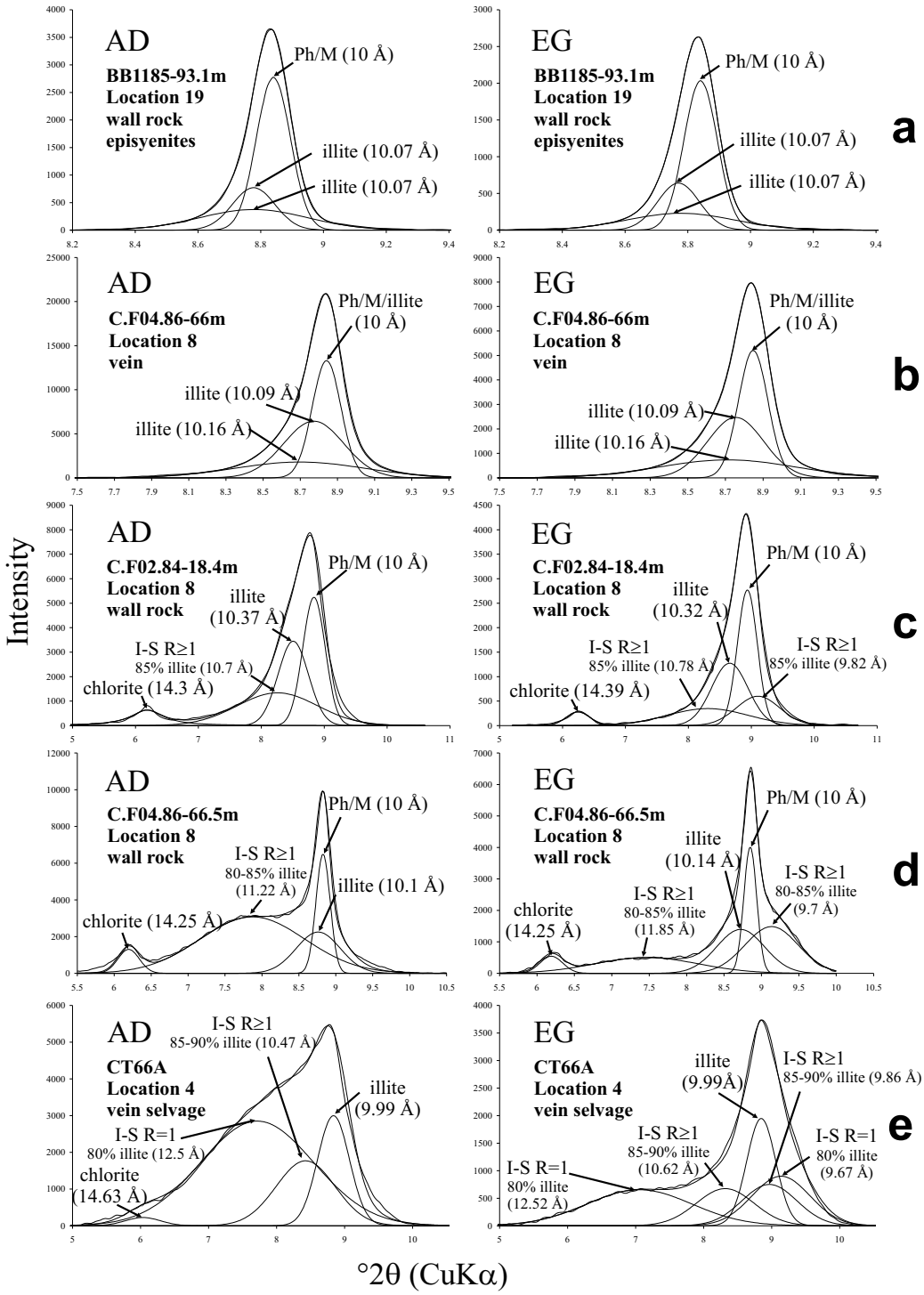

Figure 5. Decomposition of the d_{001} reflection (>99.5% fits) recorded near the 10 Å position for dioctahedral clays in air-dried (AD, left) and after ethylene glycol-solvated (EG, right) preparations from the WBF (a) and the CF granitoids (b–e). The peak-deconvolution technique (Lanson, 1997) using the DECOMPXR software (Lanson and Besson, 1992) resolves the complex basal reflection as a sum of different individual reflections in each sample. The positions of individual reflections and the estimate of the percentage of illite layers in I-S mixed layers were obtained by comparison with experimental simulations using the *Newmod*® software (Reynolds, 1985). (a) Wall-rock alteration (sample BB1185-93.1m); (b) quartz vein/breccia (sample CF04.86-66m); (c) wall-rock alteration (sample CF02.84-18.4m); (d) vein selvage (sample CF04.86-66.5m); (e) vein selvage (sample CT66-A). Ph = phengite, M =mica, I = illite, I-S = mixed-layer illite-smectite.

https://doi.org/10.1346/CCMN.2008.0560207 Published online by Cambridge University Press

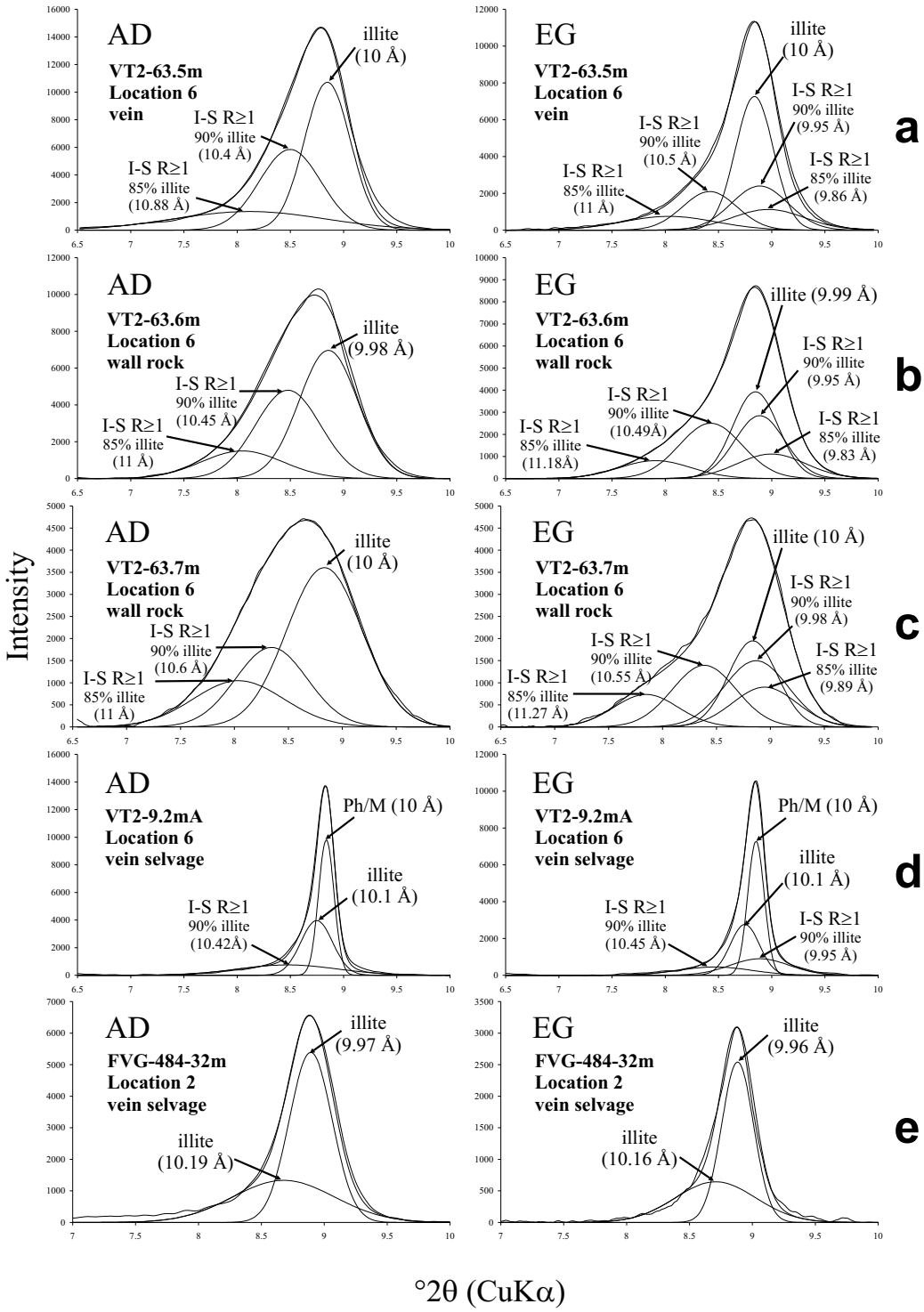

Figure 6. Decomposition of the d_{001} reflection (>99.5% fits) recorded near the 10 Å position for dioctahedral clays in air-dried (AD, left) and after ethylene glycol-solvated (EG, right) preparations of samples from the EBF (a–d) and from volcanogenic rocks (e). (a–c) Broad peaks from a sequence of sampling with increasing distance (a–c) around a 1 cm-wide quartz vein from porphyritic rocks in the EBF (samples VT2-63.5m to 63.7m); (d) narrow peak from quartz vein selvage in perthite granite from the EBF (sample VT2-9.2mA); (e) vein selvage from volcanogenic rock (sample FVG-484-32m). The positions of the peaks, estimates of the illite contents in I-S mixed layers, and the legend are the same as for Figure 5.

https://doi.org/10.1346/CCMN.2008.0560207 Published online by Cambridge University Press

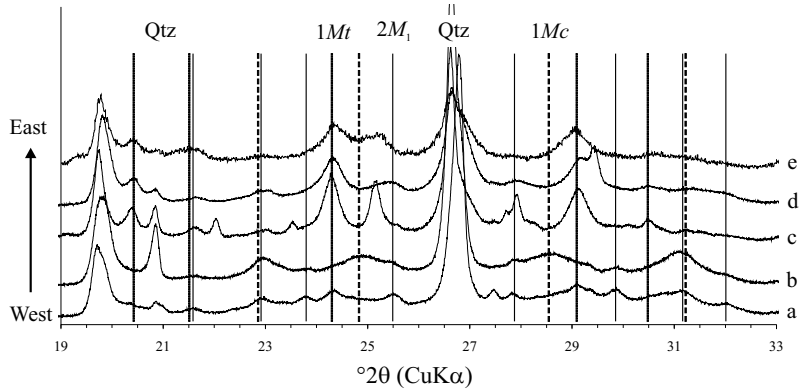

Figure 7. Three-dimensional crystallographic structure of representative analysis of dioctahedral clays (<5 μm) as a function of their location and occurrence. The positions of the diagnostic XRD reflections of 2M_1 (solid line), 1*Mt* (dotted line), and 1*Mc* (dashed line) polytypes are from Drits and McCarty (1996). (a) Wall-rock alteration, WBF (sample BB1185-93.1m); (b) quartz vein/breccia, CF (sample CF04.86-66m); (c) wall-rock alteration, CF (sample CF02.84-18.4m); (d) vein selvage from the EBF (sample VT2-63.5mA); (e) vein selvage from volcanic rocks (sample FVG-484-32m).

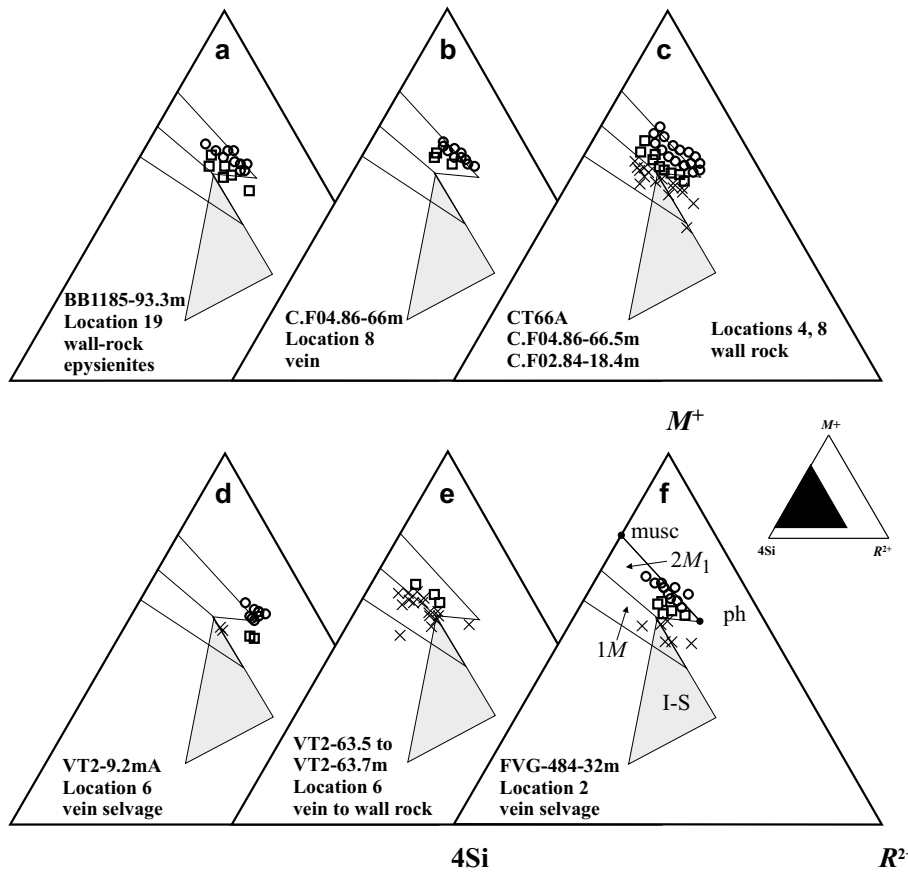

Figure 8. Representation of the chemical compositions of hydrothermal, dioctahedral clays plotted in the M^+-4Si-R^{2+} diagram (Meunier and Velde, 1989). (a) WBF (sample BB1185-93.1m); (b) vein/breccia from CF (sample CF04.86-66m); (c) vein selvage and wall-rock alteration from CF (samples CF04.86-66.5m, CF02.84-18.4m and CT66A); (d) vein selvage from EBF (sample VT2-9.2mA); (e) vein selvage in porphyritic rock from EBF (samples VT2-63.5 to 63.7m); (f) dioctahedral clays from volcanogenic rocks (samples FVG-484-32m and E017G). A typical compositional field of mixed-layer I-S is shown in gray. × = smaller interlayer charges; □ = intermediate interlayer charges; o = larger interlayer charges; musc = typical composition of muscovite; phe = maximum composition of phengite.

https://doi.org/10.1346/CCMN.2008.0560207 Published online by Cambridge University Press

Table 2. Average of microprobe analyses and structural formulae (11 oxygens) of different dioctahedral clay populations from the study area. Analyses: 1: coarse-grained phengite of wall rock alteration from WBF (sample BB1185-93.1 m); 2: fine-grained illite from wall-rock alteration associated with coarse-grained phengite from the WBF (sample BB1185-93.1 m); 3: coarse- and fine-grained phengite from quartz veins/breccia from the CF granitoids (sample C.F04.86-66 m); 4: coarse- and fine-grained illite from quartz veins/breccia from the CF granitoids (sample C.F04.86-66 m); 5: coarse- and fine-grained phengite crystallized in veinlets and alteration of magmatic biotite and feldspars from wall rock alteration from the CF granitoids (sample C.F02.84-18.4m); 6: fine-grained I-S R=1 mixed layers (up to 20% expandable component) contains the smaller interlayer charges, which cross-cuts crystals with greater interlayer charge (illite and phengite). Vein selvage from the CF granitoids (samples C.F04.66.5 m and CT66A); 7: greater interlayer charge of coarse- and fine-grained illite occur in samples with the coexistence of illite + I-S R $\geqslant$ 1 (up to 15% expandable layers). Wall-rock alteration from the CF granitoids (sample C.F02.84-18.4m). Intermediate interlayer charges between analyses 6 and 7 (0.74–0.9 per $O_{10}(OH)_2$) were identified in samples with both R=1 and R$\geqslant$1 I-S mixed layers; 8–10: phengite, I-S (up to 10% expandable layers), and illite compositional poles, respectively. Vein selvage from the EBF (sample VT2-9.2mA); 11–12: I-S R$\geqslant$1 (up to 15% expandable layers) and illite compositions from porphyritic granite, respectively, from the EBF (samples VT2-63.5 to 63.7m; 13: coarse-grained phengite from vugs in volcanic rock (sample E017G); 14–15: fine-grained poorly crystallized mixed-layer I-S (14) and well crystallized (15) illite altering feldspar crystalloclasts from vein selvage of tuffaceous rock (sample FVG-484-32m).

Analysis	1	2	3	4	5	6	7	8	9	10	11	12	13	14	15
Crystal size	C	F	C/F	C/F	C/F	F	C/F	C	C/F	C/F	F	F	C	F	F
Mineral	phe	ill	phe	ill	phe	IS R=1	ill	phe	IS R$\geqslant$1	ill	IS R$\geqslant$1	ill	phe	IS R$\geqslant$1	ill
Setting	wr	wr	v	v	wr	v	wr	v	v	v	wr	wr	v	v	v
Host rock	WBF	WBF	CF	CF	CF	CF	CF	EBF	EBF	EBF	EBF	EBF	VR	VR	VR
Na_2O	0.25	0.31	0.24	0.16	0.18	0.13	0.02	0.20	0.12	0.03	0.07	0.15	0.20	0.11	0.13
SiO_2	49.25	50.02	49.79	50.93	49.39	51.54	48.41	48.59	49.62	50.39	50.86	49.42	48.28	51.78	50.30
Al_2O_3	29.59	29.64	30.25	31.89	29.50	32.02	31.44	28.15	28.81	27.38	32.76	32.28	32.02	32.19	31.37
MgO	0.84	0.89	1.92	1.65	1.57	1.35	1.26	0.44	0.87	0.50	1.07	1.23	0.83	1.23	1.18
MnO	0.00	0.00	0.07	0.10	0.06	0.00	0.00	0.03	0.07	0.00	0.00	0.02	0.09	0.00	0.10
FeO	3.37	3.25	1.46	0.49	2.73	0.86	2.18	5.70	3.04	5.87	0.84	0.73	2.72	2.14	2.16
K_2O	10.26	8.99	10.83	10.29	10.81	8.52	10.18	10.31	8.60	9.56	9.15	9.94	10.60	9.31	10.20
CaO	0.13	0.37	0.11	0.08	0.11	0.12	0.17	0.14	0.23	0.10	0.10	0.10	0.12	0.00	0.05
TiO_2	0.27	0.48	0.22	0.12	0.17	0.00	0.00	0.05	0.13	0.04	1.20	0.11	0.16	0.25	0.23
Total	93.96	93.94	94.88	95.71	94.52	94.54	93.66	93.61	91.47	93.86	96.07	93.97	95.01	97.01	95.72
Si	3.34	3.36	3.32	3.33	3.33	3.37	3.27	3.35	3.41	3.44	3.29	3.29	3.24	3.34	3.32
Al^{IV}	0.66	0.64	0.68	0.67	0.67	0.63	0.73	0.65	0.60	0.56	0.71	0.71	0.76	0.66	0.68
Al^{VI}	1.70	1.71	1.70	1.79	1.68	1.84	1.77	1.64	1.74	1.64	1.79	1.83	1.76	1.79	1.76
Ti	0.01	0.02	0.01	0.01	0.01	0.00	0.00	0.00	0.01	0.00	0.06	0.01	0.01	0.01	0.01
Fe^{2+}	0.19	0.18	0.08	0.03	0.15	0.05	0.12	0.33	0.17	0.34	0.05	0.04	0.15	0.12	0.12
Mn	0.00	0.00	0.00	0.01	0.00	0.00	0.00	0.00	0.00	0.00	0.00	0.00	0.01	0.00	0.01
Mg	0.08	0.09	0.19	0.16	0.16	0.13	0.13	0.05	0.09	0.05	0.10	0.12	0.08	0.12	0.12
Oct. oc.	1.99	2.00	1.99	1.99	2.00	2.02	2.02	2.02	2.01	2.03	2.00	2.00	2.01	2.03	2.01
Ca	0.01	0.02	0.01	0.01	0.01	0.01	0.01	0.01	0.01	0.01	0.01	0.01	0.01	0.00	0.00
Na	0.03	0.04	0.03	0.02	0.02	0.02	0.00	0.03	0.01	0.00	0.01	0.02	0.03	0.01	0.02
K	0.89	0.77	0.92	0.86	0.93	0.71	0.88	0.91	0.75	0.83	0.76	0.84	0.91	0.77	0.86
IC	0.94	0.85	0.97	0.89	0.97	0.74	0.90	0.96	0.80	0.85	0.78	0.88	0.95	0.78	0.88
Fe/(Fe+Mg)	0.69	0.67	0.28	0.14	0.49	0.26	0.49	0.88	0.67	0.87	0.30	0.26	0.65	0.49	0.51

Oct. oc. = octahedral occupancy; IC = interlayer charge; C = coarse-grained; F = fine-grained; phe = phengite; ill = illite; IS = mixed-layer I-S.

to 0.25, due to the Tschermak substitution (Si + R^{2+} = Al^{IV} + Al^{VI}). Iron is the major component within the octahedral sheet. The average Fe/(Fe+Mg) (X_{Fe}) is 0.69 and values for Na and Mg are 0.08 and 0.03 a.p.f.u. (atoms per formula unit), respectively. Minor amounts of illite also occur in these samples. Their composition differs from those obtained in true dioctahedral micas by a smaller interlayer charge, on average 0.85 per $O_{10}(OH)_2$ (Table 2; row 2). They correspond to finer crystals identified from petrography. Iron is also the major component within its octahedral sheet and values for X_{Fe}, Mg, and Na are similar to those of phengite.

In the CF, samples with no expandable component from quartz veins and breccias (Figure 8b; sample CF04.86−66m) contain phengite and illite, as identified by XRD. Phengite occurs as coarse- and fine-grained crystals with average interlayer charge of 0.97 per $O_{10}(OH)_2$ (Table 2; row 3). Magnesium predominates over Fe in the octahedral sheet (X_{Fe} = 0.28) and Na content is 0.03 a.p.f.u. Coarse- and fine-grained illite from the same sites has an average IC of 0.89 per $O_{10}(OH)_2$, with Mg as the major divalent component in the octahedral sheet. Average values for X_{Fe} and Na are 0.14 and 0.02 a.p.f.u., respectively (Table 2, row 4).

Samples from CF with broader (>0.2º2θ FWHM) and more complex XRD profiles, containing expandable phases (samples CF02.84−18.4m, C.04.86−66.5m and CT66A) are mainly associated with wall-rock alteration, and show several chemical populations of dioctahedral clays (Figure 8c): (1) coarse- and fine-grained phengite crystallizes as veinlets and as an alteration product of igneous biotite and feldspars, with an IC value of 0.97 per $O_{10}(OH)_2$ (Table 2; row 5). Iron and Mg contents in the octahedral sheet are usually equivalent (0.15 a.p.f.u., $X_{Fe} \approx 0.5$) and the amount of Na is <0.04 a.p.f.u. (2) Dioctahedral clays with IC values of ~0.74 per $O_{10}(OH)_2$ (Table 2; row 6) from CF correspond to samples containing larger amounts of I-S R = 1 mixed layers (CT66A and CF06.86−66.5m; up to 20% of the expandable layers). They occur as fine-grained crystals associated with fillings of the wall rock through later fractures, which destabilizes the previous, coarser phases of greater IC charges. Magnesium is the dominant divalent element in the octahedral sheet, and values for X_{Fe} and Na are 0.26 and 0.02 a.p.f.u., respectively. (3) Coarse- and fine-grained crystals with IC values of ~0.9 per $O_{10}(OH)_2$ (Table 2; row 7) occur in samples rich in illite and illite-rich I-S R $\geqslant$ 1 mixed layers. The Mg contents are usually equivalent to Fe contents in the octahedral sheet (X_{Fe} = 0.49). Intermediate IC values (between 0.74 and 0.9 per $O_{10}(OH)_2$) were observed in samples with illite and I-S (R = 1 and R $\geqslant$ 1). They occur in veinlets and as alteration products of igneous minerals.

At the EBF (Figure 8d), the samples from vein selvages (VT2−9.2mA) characterized by narrow XRD profiles (0.2º2θ FWHM) contain coarse-grained phengite with average IC values of 0.96 per $O_{10}(OH)_2$ (Table 2; row 8), associated with the highest values of octahedral Fe (X_{Fe}= 0.88), and Na of <0.03 a.p.f.u. Minor amounts of coarse- and fine-grained illite ± illite-rich I-S mixed layers were also analyzed in the same sample as shown by some analyses which give IC values between 0.80 and 0.87 per $O_{10}(OH)_{20}$ (Table 2; rows 9 and 10).

Samples containing dioctahedral, potassic phyllosilicates with broader and complex peaks (>0.2º2θ FWHM) rich in I-S R $\geqslant$ 1 mixed layers (VT2−63.5 to 63.7m; up to 15% expandable layers) from wall-rock alteration have variable IC between 0.78 and 0.88 per $O_{10}(OH)_2$ (Figure 8e; Table 2, rows 11 and 12). Magnesium is the major divalent element in the octahedral sheet and the X_{Fe} value (0.30) and amount of Na (<0.02 a.p.f.u.) are similar in both populations.

Dioctahedral clays of vein selvages from the volcanic rocks also consist of phengite and illite (Figure 8f). Phengite corresponds to average interlayer charges of 0.95 per $O_{10}(OH)_2$ (Table 2, row 13). Magnesium is the major divalent component of the octahedral sheet and the Na content is <0.03 a.p.f.u. They are also associated with the coarser crystals filling vugs in the volcanic rocks that were rarely found during sampling (sample E017G). Analysis of fine-grained crystals (from alteration of crystalloclasts from wall-rock alteration of stockworks (sample FVG-484)) shows two populations with average IC values of 0.78 and 0.88 per $O_{10}(OH)_2$. The former value (Table 2, row 14) corresponds to very small quantities (<5%) of smectite in illite-rich I-S mixed layers that were not detected in XRD data and the latter value (Table 2, row 15) corresponds to the two illite populations recognized during decomposition of XRD patterns (Figure 5e). Magnesium and Fe contents in the octahedral sheet ($X_{Fe} \approx 0.50$) and the amount of Na (<0.02 a.p.f.u.) are quite similar in these clay populations.

INTERPRETATION AND DISCUSSION

In this study, the data obtained from alteration petrography, crystal structure, and crystal chemistry of the potassic dioctahedral phyllosilicates, usually reported as sericite in similar fracture-controlled hydrothermal systems, suggest that the Lavras do Sul district was affected by a multistage, hydrothermal event. The main and widespread alteration stage is related to Au deposition concomitantly with crystallization of secondary quartz, sulfides, and sericite in veins and associated altered wall rocks. The sericitic alteration is heterogeneous in term of clay mineralogy, represented by several dioctahedral phyllosilicates identified as phengite, illite, and illite-rich I-S R $\geqslant$ 1 mixed layers (locally R = 1).

Spatial and temporal evolution of dioctahedral clay minerals

The spatial and temporal distributions of the alteration stages identified in the study area, coupled with data from previous works, are illustrated in Figure 9.

https://doi.org/10.1346/CCMN.2008.0560207 Published online by Cambridge University Press

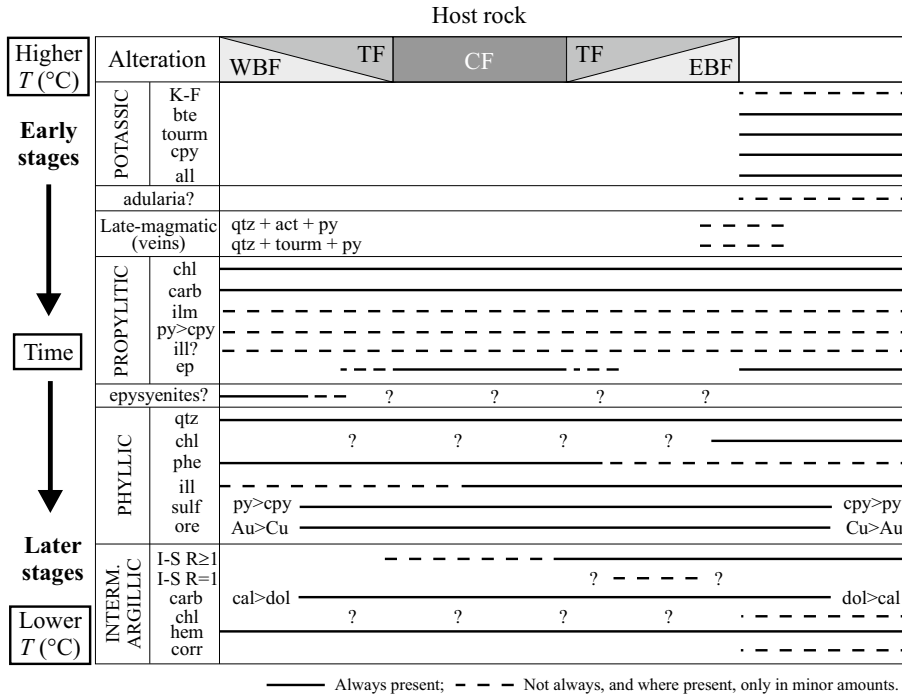

Figure 9. Spatial and temporal distribution of the alteration assemblages and stages identified in the study area. Abbreviations: K-F (alkali feldspar), bte (biotite), tourm (tourmaline), cpy (chalcopyrite), all (allanite), qtz (quartz), act (actinolite), py (pyrite), chl (chlorite), cal (calcite), ilm (ilmenite), ill (illite), ep (epidote), phe (phengite), sulf (sulfides), carb (carbonate), hem (hematite), and corr (corrensite). Adularia and episyenite positions are approximate.

Phengite, illite, and I-S mixed layers occur in most of the altered host rocks. Pure phengite was recognized by low FWHM values measured on <5 μm clays ($\leqslant 0.2°2\theta$), non-expandable d_{001} X-ray reflections after EG solvation, IC >0.9 per $O_{10}(OH)_2$, and coarse-grained, hexagonal crystals of the $2M_1$ polytype. Phengite is best developed in coarse-grained, primary growth (comb) quartz + pyrite ± Au veins and altered wall rocks from the WBF (Table 1; mainly BB samples), where very minor amounts of illite are observed locally.

The occurrence of phengite was followed by the crystallization of fine-grained dioctahedral clays as time progressed, proven by overgrowth, cross-cutting relationships and recrystallization textures (Figure 2) towards the eastern zones of the granitic complex and the volcanic area, where narrow XRD profiles (<5 μm) are rarely observed (Figure 3).

X-ray diffraction data from samples with superimposition of other dioctahedral clay populations show wider FWHM values ($\geqslant 0.2°2\theta$). The mineralogy of the individual peaks that constitute these wider d_{001} X-ray reflections on <5 μm clays was obtained only after XRD decompositions. Those X-ray reflections are best expressed in samples associated with fine-grained, primary growth (colloform, crustiform, zonal), recrystallization (flamboyant), and replacement (saccharoidal and lattice-bladed textures) quartz + pyrite + chalcopyrite ± Au ± Cu veins, breccias, and altered wall rocks from the CF, TF, EBF, and from the volcanic area (Table 1), where phengite is absent or poorly expressed.

Illite was recognized by non-expandable d_{001} XRD reflections after EG solvation, with an IC value of between 0.85 and 0.89 per $O_{10}(OH)_2$ and coarse- to fine-grained lath-like crystals of both $2M_1$ and $1M$ polytypes. Mixed-layer I-S minerals were identified by the presence of an expandable component (shift of the d_{001} reflections after EG solvation) and lath-like, fine-grained crystals. X-ray patterns of these minerals are compatible with ordered, R ⩾ 1, illite-rich (80–90%) I-S mixed layers (IC of ~0.8 per $O_{10}(OH)_2$) and in very minor amounts (samples CT66A and CT66B) with regularly ordered, R = 1, I-S mixed layers (up to 75% illite) characterized by a large superstructure close to 25–26 Å at AD (IC of ~0.74 per $O_{10}(OH)_2$).

Quartz + sulfides + phengite and quartz + illite + illite-rich I-S mixed-layer assemblages are characteristic of phyllic and intermediate argillic alteration facies described in porphyry-type environments (Creasey, 1959; Lowell and Guilbert, 1970; Beane, 1982) and in deeper zones of epithermal deposits (*e.g.* Hedenquist *et al.*, 1998), respectively. In other words, phyllic alteration (characterized by phengite) predominates in the WBF (BB samples, location 19), whereas the intensity of the intermediate argillic alteration (which is superimposed on the phyllic paragenesis) significantly increases towards the CF (CF samples, location 8), the

https://doi.org/10.1346/CCMN.2008.0560207 Published online by Cambridge University Press

EBF (VT samples, location 6), and the volcanic area (FVG samples, location 2), with increasing occurrence of illite + R $\geqslant$ 1 I-S mixed layers.

Chlorite is associated with fine-grained illite + R $\geqslant$ 1 I-S mixed layers in fine-grained, primary growth (+recrystallization and replacement), quartz veins, breccias, and wall-rock alteration (EBF and in the volcanic area, locations 1 to 6) that cross-cut the previous alteration stages dominated by dioctahedral clays. When chlorite, illite, and I-S mixed layers are associated with corrensite, carbonate, and specular hematite in later fractures, it constitutes the argillic alteration stage, as previously assumed (Mexias *et al.* 1990).

The clay mineral zonation observed does not reflect exhumation of different levels of exposure of a metamorphosed terrain, because the main granitic complex is intrusive in an older metamorphic terrain (~750–700 Ma; Figure 1) in its western and southwestern borders. The spatial variation of the crystal characteristics (grain size and shape, FWHM values of d_{001} X-ray reflections, polytypes and crystal chemistry) at a regional scale suggests that clay minerals that outcrop in the eastern part of the mining district crystallized at lower thermal conditions (lower rank structural features and smaller IC values) than those of the western part (higher rank structural features and greater IC values). This is also suggested by the quartz textural association in the hydrothermal veins that are rather characteristic of shallow epithermal systems in the EBF (fine-grained, primary growth, recrystallization, and replacement) and rather characteristic of porphyry systems in the WBF and CF (coarse-grained, primary growth).

The spatial distribution of the dioctahedral clay minerals could be explained by the asymmetric exhumation of a large hydrothermal system that has been tilted to expose its deeper parts in the western zones and its shallower parts in the eastern zones of the study area, even if the area considered here (12 km × 5 km) is larger than those usually observed for a single porphyry system. Another possibility is the superimposition of two distinctive hydrothermal systems, not exposed now. According to Sasada (2000), intrusive bodies associated with porphyry copper systems generally consist of several intrusive units. K/Ar determinations of the different dioctahedral clay minerals might not distinguish the age of the different alteration stages, because the standard deviation on the chronological data may exceed the total duration of the hydrothermal activity around porphyry stocks (commonly <1 Ma).

The occurrence of potassic alteration along the contact between the granitic and volcanic rocks (Mexias *et al.*, 1990) may indicate the transition of tilted porphyry to epithermal deposit with telescoping of hydrothermal alteration features, shown by variations in the clay mineralogy and quartz-vein textures.

The occurrence of breccias, microcataclasites, quartz subgrains, and intragranular fractured zones, as well as recrystallization and replacement quartz textures along the mineralized veins towards the eastern zones of the mining district, indicate multiple stages of seismic activity and related hydrothermal alteration. The fluid flows associated with the dioctahedral clay distribution in the Lavras granitic complex are entirely controlled by a fracture network related to a structural event that postdates the emplacement of the granitic complex. The main mineralized structures consist of conjugate fracture systems whose directions presumably reflect a palaeostress field. In most porphyry deposits, the phyllic to argillic alteration zones occupy a relatively small volume. Even at large deposits such as Bingham, the maximum diameter of the altered zone reaches 1700 m (Parry *et al.*, 2002) and, in general, the fractures associated with porphyry deposits typically do not extend more than 4 km from the porphyry center (Titley, 1982). However, in highly fracture-controlled deposits like those from the study area, the hydrothermal alteration may concentrate around longer structural sites.

Influence of temperature on the structural-chemical variations of dioctahedral phyllosilicates

The results obtained in this study allow us to estimate the *P-T* conditions of the hydrothermal alteration associated with the major mineralized zones. Clay thermometry based on chemical compositions is always controversial because the compositional variations of clay particles are frequently more representative of mixing of different clay mineral phases (*i.e.* non-expandable clay minerals and expandable mixed-layer clay minerals) than of true crystal chemical variation in a discrete crystal. Interstratified minerals are considered as metastable precursors of the end-member minerals of both di- and trioctahedral conversion series (Essene and Peacor, 1995). It can be exemplified by the wide range of interlayer charges (intermediate IC between end-members of clay populations) observed in chemical analyses of samples containing both illite and I-S mixed layers (Table 2; Figure 8). However, crystal structural parameters (FWHM, degree of order-disorder in the stacking sequence) are considered to be good markers of the range of temperature for crystallization of dioctahedral clays (Merriman and Peacor, 1999; Tillick *et al.*, 2001).

The temperatures recorded by the observed clay mineralogy are near 300ºC for phengite (Beaufort *et al.*, 1990) and illite (Simmons and Browne, 1998) and between 160 and 200ºC for illite-rich ordered (R $\geqslant$ 1) I-S mixed layers (Velde, 1985; Nadeau and Reynolds, 1981); these temperatures agree with chlorite crystallization temperatures. Regularly ordered (R = 1) I-S mixed layers, observed locally, can crystallize at slightly lower temperatures, between 120 and 180ºC (Nadeau and Reynolds, 1981; Horton, 1985).

Based on the literature data, the regional-scale differences in the dioctahedral clay mineralogy may

https://doi.org/10.1346/CCMN.2008.0560207 Published online by Cambridge University Press

reflect variation of temperature from ~300ºC for phengite from the western zone of the granitic complex (WBF-samples, Table 1; FWHM between 0.14 and 0.2º2θ) to temperatures of <180ºC in samples with illite-rich I-S (R ⩾ 1) with greater amounts of expandable layers in the central and eastern zones (CF and EBF samples, Table 1; FWHM between 0.23 and 0.89º2θ). Those temperatures agree with the thermal conditions for coarse-grained, primary growth, and fine-grained, primary growth (+ recrystallization and replacement), quartz crystallization associated with phengite (phyllic alteration), and illite/I-S mixed layers (intermediate argillic alteration), respectively. Although the overall distribution of clay minerals is consistent with temperature as a controlling variable, small heterogeneities in the distribution of clay minerals were controlled by the water/rock ratio. Indeed, various water/rock ratios may have an impact on the dioctahedral clay mineralogy as shown in samples VT-63.5 to 63.8m from porphyritic syenogranites from the EBF, where a discrete structural evolution of illite + illite-rich, I-S mixed layers around a 1 cm-wide quartz vein was observed. With increasing distance from the vein (up to 30 cm) and consequently with decreasing water/rock ratio, the XRD intensity of the non-expandable component decreases, accompanied by a slight increase in the amounts of expandable component within the I-S mixed layer (Table 1; FWHM from 0.54 to 0.79º2θ). However, at the scale of the granitic complex, this parameter can be ignored if we compare sericite minerals developed only in quartz veins and breccias.

Fluid inclusion (FI) data of veins and wall rocks from the Lavras do Sul region (Bongiolo, 2007) agree with those obtained using mineralogical parameters. At the WBF (location 19), quartz from wall-rock alteration where phengite-illite predominates, shows mainly secondary, two-phase aqueous inclusions (T_h = 210–365ºC; 0.7–13 wt.% NaCl eq.). Quartz crystals, from wall-rock alteration at the EBF (location 6), where illite + illite-rich I-S (R = 1) predominate, show abundant primary (T_h ⩽60 to 170ºC; 0.3–20 wt.% NaCl eq.) and secondary (T_h ⩽60 to 270ºC; 1–20 wt.% NaCl eq.) low-temperature single- to two-phase aqueous FI. Primary FI from veins at the EBF are also associated with single- to two-phase aqueous inclusions (T_h ⩽60–200ºC; 3–10 wt.% NaCl eq.), with no petrographic evidence of boiling.

Relation of sampling with ore mineralization

Prospecting reports from bore-hole sampling by Brazilian public agencies show that samples analyzed in this work have highly variable gold and copper contents.

Samples rich in coarse-grained, hexagonal, $2M_1$-phengite, with very minor amounts of fine-grained, lath-like, 1*M* illite (FWHM ⩽0.2º2θ; IC_{phe} = 0.94 and IC_{ill} = 0.85) from the WBF (location 19; BB samples) have 1 g/t of Au. The association of coarse- to fine-grained, hexagonal to lath-like crystals of $2M_1$ to 1*M* phengite to illite (FWHM = 0.23º2θ; IC_{phe}= 0.97 and IC_{ill} = 0.89) from the CF (location 8; sample CF04.86–66m) also contain ~1 g/t of Au. Samples from the EBF (location 6; VT2–9.2mA), rich in coarse-grained, hexagonal, $2M_1$ phengite (FWHM = 0.23º2θ; IC_{phe} = 0.96) that were superimposed by fine-grained, lath-like 1*M* illite and R ⩾ 1 I-S mixed layers (IC_{ill} = 0.85 and $IC_{I\text{-}S}$ = 0.80), as well as samples associated exclusively with the latter minerals (VT2–63.5 to 63.8m; FWHM = 0.54 to 0.79º2θ; IC_{ill} = 0.88 and $IC_{I\text{-}S}$ = 0.78), do not contain large amounts of ore (<0.3 g/t Au and <0.02% Cu, respectively).

Samples from the EBF associated with later, chlorite-rich (+I-S R ⩾ 1 mixed layers; FWHM = 0.48º2θ), quartz + chalcopyrite ± pyrite ± calcite infilling breccias (sample VT2-44.8m) and its wall-rock alteration have larger Cu contents (up to 1.3%). In samples from the volcanogenic area (FVG samples, location 2), copper also predominates over gold contents (1.5 g/t of Au and 1% of Cu). In those rocks, ore is associated with chlorite-rich quartz + fine-grained, lath-like, 1*M* illite and I-S R ⩾ 1 mixed layers (FWHM = 0.18 to 0.33º2θ; IC_{ill} = 0.88 and $IC_{I\text{-}S}$ = 0.78) + sulfides ± calcite veins and its wall-rock alteration.

Available gold and copper values suggest that in the granitic rocks, gold is associated with phengite-rich veins and wall rocks, and that illite-I-S overprint may have modified the original grade in and near fracture zones. The volcanogenic area contains the larger Cu contents associated with chlorite-rich veins that can also be found in the same structures along the contact between granitic and volcanic rocks.

CONCLUSIONS

This study establishes that the dioctahedral phyllosilicates that characterize the alteration associated with gold mineralization in the Lavras do Sul hydrothermal system comprise mixtures of phengite, illite, and illite-rich I-S mixed layers that cannot be considered as a product of a single alteration stage. These minerals are ubiquitous throughout the study area, but their crystallization is not synchronous everywhere.

Dioctahedral phyllosilicates show textural, structural, and chemical evolution, from coarse-grained $2M_1$ phengite-illite at the western zones of the granitic complex, to fine-grained 1*M* illite to R ⩾ 1 illite-rich I-S mixed layers towards the eastern granitoids and volcanogenic rocks. Petrographic observations also confirm that phengite crystallized earlier than illite and I-S mixed layers. Those observations allow us to propose that deeper zones within the main granitic body are situated in its western border and constitute a phyllic alteration (phengite-rich), usually crystallized under higher thermal conditions (perhaps influenced by mag-

https://doi.org/10.1346/CCMN.2008.0560207 Published online by Cambridge University Press

matic dominant fluids). In the WBF, phyllic alteration was only locally affected by the later crystallization of lower-rank dioctahedral clay assemblages identified as an intermediate argillic alteration (illite and illite-rich I-S mixed layers). Thus, the illite + illite-rich I-S mixed layers assemblage crystallized later, towards eastern zones of the study area, under influence of low-temperature fluids (perhaps meteoric-water dominant) that flowed through the same paleoconduits as the earlier assemblages. The dominance of chloritic breccia near the contact between the granitic and volcanogenic rocks implies an inversion of the fluid flow through the major fractured zones.

No clay zonation has been detected across the granitic complex. The distribution of clay minerals in and near fractured zones indicates that hydrothermal alteration cannot relate solely to emplacement of the granitic complex; alteration must also relate to the structural event that formed the fracture network that postdates granite emplacement. The occurrence of high-temperature alteration (potassic alteration or high-temperature veins) and telescoping in vein-controlled and wall-rock alteration features (clay mineralogy and quartz textures) along the contact between the granitic and volcanic rocks may indicate shallower levels of a porphyry to epithermal deposit.

Available Au and Cu values show that in the granitic rocks, Au is associated with phengite-rich veins and wall rocks, but illite-I-S overprint may have modified the original grade in and near fracture zones. The volcanic area contains the larger Cu contents associated with chlorite-rich veins that can be also found in the same structures along the contact between granitic and volcanic rocks.

ACKNOWLEDGMENTS

This study was partly funded by CNPq (project 465219/2000-4) and PRONEX/CNPq (project 662179/1997-8). The authors thank Companhia Brasileira do Cobre (CBC), Companhia Riograndense de Mineração (CRM), Seahawk Minerals Limited, and IAMGOLD Corporation for providing access to drill-core samples. We thank Jeffrey L. Mauk, Ray Ferrell, and an anonymous reviewer for providing constructive comments on an earlier version of this manuscript. Everton M. Bongiolo also thanks CNPq for the PhD scholarship and the CAPES-COFECUB project (349-01/2003).

REFERENCES

Babinski, M., Chemale Jr., F., Hartmann, L.A., Van Schmus, W.R., and Silva, L.C. (1996) Juvenile accretion at 750–700 Ma in southern Brazil. *Geology*, **24**, 439–442.

Beane, R.E. (1982) Hydrothermal alteration in silicate rocks, southwestern North America. Pp.117–137 in: *Advances in Geology of the Porphyry Copper Deposits* (S.R. Titley, editor). SNA University of Arizona Press, Tucson, Arizona.

Beaufort, D., Westercamp, D., Legendre, O., and Meunier, A. (1990) The fossil hydrothermal system of Saint Martin, Lesser Antilles: Geology and lateral distribution of alterations. *Journal of Volcanology and Geothermal Research*, **40**, 219–243.

Bish, D.L. and Reynolds Jr., R.C. (1989) Sample preparation for X-ray diffraction. Pp. 73–99 in: *Modern Powder Diffraction* (D.L. Bish and J.E. Post, editors). Mineralogical Society of America, Washington, D.C.

Bongiolo, E.M. (2007) Integração de dados mineralógicos, isótopos estáveis (O, H) e porosidade de rochas (^{14}C-PMMA) no reconhecimento da evolução da alteração no sistema hidrotermal de Lavras do Sul/RS, Brasil. PhD thesis, Porto Alegre, UFRGS, Brazil, 189 pp.

Bouchet, A., Meunier, A., and Sardini, P. (2001) *Minéraux argileux – structures cristallines – identification par diffraction de rayons X*. With CD-ROM. TotalFinaElf Editions, 136 pp.

Bril, H., Papapanagiotou, P., Patrier, P., Lenain, J.F., and Beaufort, D. (1996) Fluid-rock interaction in the geothermal field of Chipilapa (El Salvador): Contribution of fluid inclusion data. *European Journal of Mineralogy*, **8**, 515–531.

Chemale Jr., F., Hartmann, L.A., and Silva, L.C. (1995) Stratigraphy and tectonism of Brasiliano Cycle in southern Brazil. *Communications of Geological Survey of Namibia*, **10**, 151–166.

Creasey, S.C. (1959) Some phase relations in hydrothermally altered rock of porphyry copper deposits. *Economic Geology*, **54**, 351–373.

De Liz, J.D., Lima, E.F., Nardi, L.V.S., Hartmann, L.A., Sommer, C.A., and Gonçalves, C.R.H. (2004) Aspectos petrográficos e composicionais do sistema multi-intrusivo da associação shoshonítica Lavras do Sul (RS) e seu potencial para mineralizações de ouro e sulfetos. *Revista Brasileira de Geociências*, **34**, 539–552.

Drits, V.A. and McCarty, D.K. (1996) The nature of diffraction effects from illite and illite-smectite consisting of interestratified trans-vacant and cis-vacant 2:1 layers: A semiquantitative technique for determination of layer-type content. *American Mineralogist*, **81**, 852–863.

Dowling, K. and Morrison, G.W. (1989) Application of quartz textures to the classification of gold deposits using North Queensland examples. *Economic Geology Monograph*, **6**, 342–355.

Essene, E.J. and Peacor, D.R. (1995) Clay mineral thermometry. A critical perspective. *Clays and Clay Minerals*, **43**, 540–553.

Flexser, S. (1991) Hydrothermal alteration and past and present thermal regimes in the western moat of Long Valley caldera. *Journal of Volcanology and Geothermal Research*, **48**, 303–318.

Franchini, M., Impiccini, A., Meinert, L., Grathoff, G., and Schalamuk, I.B.A. (2007) Clay mineralogy and zonation in the Campana Mahuida porphyry Cu deposit, Neuquén, Argentina: implications for porphyry Cu exploration. *Economic Geology*, **102**, 27–54.

Gastal, M.C.P. and Lafon, J.M. (1998) Gênese e evolução dos granitóides metaluminosos de afinidade alcalina da porção oeste do escudo Sul-riograndense: Geoquímica e isótopos de Rb-Sr e Pb-Pb. *Revista Brasileira de Geociências*, **28**, 11–28.

Gastal, M.C.P., Lafon, J.M., and Koester, E. (2003) Sr-Nd-Pb isotopes for minettes and granitoids from the Lavras do Sul Intrusive Complex, RS. Pp. 564–567 in: *IV South American Symposium on Isotope Geology*, Salvador, Short Papers, **2**.

Harvey, C.C. and Browne, P.R.L. (1991) Mixed-layer clay geothermometry in the Wairakei Geothermal Field, New Zealand. *Clays and Clay Minerals*, **39**, 614–621.

Hedenquist, J.W., Arribas Jr., A., and Reynolds, T.J. (1998) Evolution of an intrusion-centered hydrothermal system: Far Southeast-Lepanto porphyry and epithermal Cu-Au deposits, Philippines. *Economic Geology*, **93**, 373–404.

Horton, D.G. (1985) Mixed-layer illite/smectite as a paleotemperature indicator in the Amethyst vein system, Creede District, Colorado, USA. *Contributions to Mineralogy and Petrology*, **91**, 171–179.

Inoue, A. (1995) Formation of clay minerals in hydrothermal environments. Pp. 268–329 in: *Origin and Mineralogy of Clays* (B. Velde, editor). Springer-Verlag, New York.

Jin, Z., Zhu, J., Ji, J., Li, F., and Lu, X. (2002) Two origins of illite at the Dexing porphyry Cu deposit, East China: implications for ore-forming fluid constraint on illite crystallinity. *Clays and Clay Minerals*, **50**, 381–387.

Kaul, P.F.T. and Rheinheimer, D. (1974) *Projeto Ouro no Rio Grande do Sul e Santa Catarina*. Relatório Final em Convênio CPRM/DNPM, Brazil, 290 pp.

Lanson, B. (1997) Decomposition of experimental X-ray diffraction patterns (profile fitting). A convenient way to study clay minerals. *Clays and Clay Minerals*, **45**, 132–146.

Lanson, B. and Besson, G. (1992) Characterization of the end of smectite-to-llite transformation; decomposition of X-ray patterns. *Clays and Clay Minerals*, **40**, 40–52.

Lanson, B. and Champion, D. (1991) The I-S-to-illite reaction in the late stage diagenesis. *American Journal of Science*, **291**, 473–596.

Lima, E.F. and Nardi, L.V.S. (1998) The Lavras do Sul Shoshonitic association: implications for origin and evolution of neoproterozoic shoshonitic magmatism in southernmost Brazil. *Journal of South American Earth Sciences*, **11**, 67–77.

Lowell, J.D and Guilbert, J.M. (1970) Lateral and vertical alteration – mineralization zoning in porphyry ore deposits. *Economic Geology*, **69**, 373–408.

Mas, A., Patrier, P., Beaufort, D., and Genter, A. (2003) Clay-mineral signatures of fossil and active hydrothermal circulations in the geothermal system of the Lamentin Plain, Martinique. *Journal of Volcanology and Geothermal Research*, **124**, 195–218.

Merriman, R.J. and Peacor, D.R. (1999) Very low grade metapelites: mineralogy, microfabrics and measuring reaction progress. Pp. 10–60 in: *Low-grade Metamorphism* (M. Frey and D. Robinson, editors). Blackwell Publishing, Oxford, UK.

Meunier, A. (2003) *Argiles*. CPI-GB Science Publisher, Paris, 433 pp.

Meunier, A. and Velde, B. (1989) Solid solutions in I-S mixed-layer minerals and illite. *American Mineralogist*, **74**, 1106–1112.

Meunier, A. and Velde, B. (2004) *Illite: Origins, Evolution, and Metamorphism*. Springer-Verlag, Berlin, 286 pp.

Mexias, A.S., Formoso, M.L.L., Meunier, A., and Beaufort, D. (1990) O sistema hidrotermal fóssil de Volta Grande – Lavras do Sul/RS. Parte I – Petrografia do hidrotermalismo. *Geochimica Brasiliensis*, **4**, 139–157.

Mexias, A.S., Berger, G., Gomes, M.E.B., Formoso, M.L.L., Dani, N., Frantz, J.C., and Bongiolo, E.M. (2005) Geochemical modelling of gold precipitation conditions in the Bloco do Butiá Mine, Lavras do Sul/Brazil. *Anais da Academia Brasileira de Geociências*, **77**(3), 1–12.

Nadeau, P.H. and Reynolds, C.R. (1981) Burial and contact metamorphism in the Mancos Shale. *Clays and Clay Minerals*, **29**, 249–259.

Nardi, L.V.S. (1984) Geochemistry and petrology of the Lavras Granite Complex, RS, Brazil. PhD thesis, Department of Geology, University of London, UK, 268 pp.

Nardi, L.V.S. and Lima, E.F. (2000) O magmatismo shoshonítico e alcalino da Bacia do Camaquã – RS. Pp. 119–131 in: *Geologia e Estratigrafia do Rio Grande do Sul* (M. Holz and L.F. De Ros, editors). Editora Gráfica da UFRGS, Porto Alegre, Brazil.

Norton, D. and Knight, J. (1977) Transport phenomena in hydrothermal systems: cooling plutons. *American Journal of Science*, **277**, 937–981.

Parry, W.T., Jasumback, M., and Wilson, P.N. (2002) Clay mineralogy of phyllic and intermediate argillic alteration at Bingham, Utah. *Economic Geology*, **97**, 221–239.

Patrier, P., Papapanagiotou, P., Beaufort, D., Traineau, H., Bril, H., and Rojas, J. (1996) Role of permeability versus temperature in the distribution of the fine (<0.2 μm) clay fraction in the Chipilapa geothermal system (El Salvador). *Journal of Volcanology and Geothermal Research*, **72**, 101–120.

Reischl, J.L. (1980) Mineralizações auríferas associadas ao Complexo Granítico Lavras do Sul - RS. Pp. 700–1712 in: *Congresso Brasileiro de Geologia 32*, Camboriú, Anais. Sociedade Brasileira de Geociências, **3**, Brazil.

Reischl, J.L. (1998) *Diagnóstico do potencial mineral do município de Lavras do Sul/RS. Public repport*. Minerar Consultoria e Projetos Ltda, 1 CD-ROM, Brazil.

Remus, M.V.D., Hartmann, L.A., McNaughton, N.J., and Groves, D.I. (2000) Distal magmatic-hydrothermal origin for the Camaquã Cu (Au-Ag) and Santa Maria Pb, Zn (Cu-Ag) Deposits, Southern Brazil. *Gondwana Research*, **3**, 155–174.

Reyes, A.G. (1990) Petrology of the Philippine geothermal systems and the application of alteration mineralogy to their assessment. *Journal of Volcanology and Geothermal Research*, **43**, 279–309.

Reynolds, R.C. (1980) Interstratified minerals. Pp. 249–274 in: *Crystal Structures of Clay Minerals and their X-ray Identification* (G.W. Brindley and G. Brown, editors). Monograph **5**, Mineralogical Society of London.

Reynolds, R.C. (1985) *Description of program NEWMOD for the calculation of one-dimensional X-ray diffraction patterns of mixed-layered clays*. Department of Earth Sciences, Dartmouth College, Hanover, New Hampshire, USA.

Ribeiro, M. (1983) Informes sobre a Formação Maricá. *Iheringia, Série Geologia*, **9**, 3–50.

Sasada, M. (2000) Igneous-related active geothermal system versus porphyry copper hydrothermal system. Pp. 1691–1693 in: *Proceedings of the World Geothermal Congress*. Kyushu-Tohoku, Japan.

Simmons, S.F., Arehart, G., Simpson, M.P., and Mauk, J.L. (2000) Origin of massive calcite in the Golden Cross Low-sulphidation, epithermal Au-Ag Deposit, New Zealand. *Economic Geology*, **95**, 99–112.

Środoń, J., Elsass, F., McHardy, W.J., and Morgan, D.J. (1992) Chemistry of illite/smectite inferred from TEM measurements of fundamental particles. *Clay Minerals*, **27**, 137–158.

Tillick, D.A., Peacor, D.R., and Mauk, J.L. (2001) Genesis of dioctahedral phyllosilicates during hydrothermal alteration of volcanic rocks: I. The Golden Cross epithermal ore deposit, New Zealand. *Clays and Clay Minerals*, **49**, 126–140.

Titley, S.R. (1982) The style and progress of mineralization and alteration in porphyry copper systems. Pp. 93–166 in: *Advances in Geology of the Porphyry Copper Deposits, southwestern North America* (S.R. Titley, editor). University of Arizona Press, Tucson, Arizona.

Velde, B. (1985) *Clay Minerals: a Physico-Chemical Explanation of their Occurrence*. Developments in Sedimentology **40**, Elsevier, Amsterdam, 427 pp.

(*Received 1 November 2006; revised 21 December 2007; Ms. 1234; A.E. R.E. Ferrell*)